Neurobiology of Disease 94 (2016) 139–156

Contents lists available at ScienceDirect

Neurobiology of Disease

journal homepage: www.elsevier.com/locate/ynbdi

Calcineurin β protects brain after injury by activating the unfolded protein response

Yanan Chen [a], Deborah M. Holstein [a], Sofia Aime [b], Mariana Bollo [b,*], James D. Lechleiter [a,c,*]

[a] Department of Cellular and Structural Biology, University of Texas Health Science Center at San Antonio, TX, USA
[b] Instituto de Investigación Médica M y M Ferreyra, INIMEC-CONICET, Universidad Nacional de Córdoba, Córdoba, Argentina
[c] Center for Biomedical Neuroscience, University of Texas Health Science Center at San Antonio, TX, USA

ARTICLE INFO

Article history:
Received 4 May 2016
Revised 15 June 2016
Accepted 17 June 2016
Available online 19 June 2016

Keywords:
Calcium
Stress
Ischemia
Traumatic brain injury
Endoplasmic reticulum

ABSTRACT

The Ca^{2+}-dependent phosphatase, calcineurin (CN) is thought to play a detrimental role in damaged neurons; however, its role in astrocytes is unclear. In cultured astrocytes, CNβ expression increased after treatment with a sarco/endoplasmic reticulum Ca^{2+}-ATPase inhibitor, thapsigargin, and with oxygen and glucose deprivation, an *in vitro* model of ischemia. Similarly, CNβ was induced in astrocytes *in vivo* in two different mouse models of brain injury - photothrombotic stroke and traumatic brain injury (TBI). Immunoprecipitation and chemical activation dimerization methods pointed to physical interaction of CNβ with the unfolded protein response (UPR) sensor, protein kinase RNA-like endoplasmic reticulum kinase (PERK). In accordance, induction of CNβ resulted in oligomerization and activation of PERK. Strikingly, the presence of a phosphatase inhibitor did not interfere with CNβ-mediated activation of PERK, suggesting a hitherto undiscovered non-enzymatic role for CNβ. Importantly, the cytoprotective function of CNβ was PERK-dependent both *in vitro* and *in vivo*. Loss of CNβ *in vivo* resulted in a significant increase in cerebral damage, and correlated with a decrease in astrocyte size, PERK activity and glial fibrillary acidic protein (GFAP) expression. Taken together, these data reveal a critical role for the CNβ-PERK axis in not only prolonging astrocyte cell survival but also in modulating astrogliosis after brain injury.

1. Introduction

After brain injury, such as cerebral ischemic stroke or traumatic brain injury (TBI), the long-term fate of cells is determined not only by the brain's initial vulnerability to the primary injury, but also by its ability to mount a competent cellular defense during the secondary injury phase. The central role of calcium and its downstream targets, such as the highly conserved Ca^{2+}/calmodulin-dependent serine/threonine protein phosphatase, calcineurin (CN) has been particularly studied in neurons. CN exists as a heterodimer consisting of a catalytic subunit (CN-A) and a regulatory subunit (CN-B) (Klee & Krinks, 1978). CN-A is encoded by three genes (PPP3CA, PPP3CB and PPP3CC genes); the products of PPP3CA and PPP3CB are CN-A isoform α and β, which share 81% sequence homology and are highly abundant in mammalian brain tissue (Kuno et al., 1992), particularly in the striatum and the CA1 region of the hippocampus (Polli et al., 1991). Here, we will refer to CN-Aα/B and CN-Aβ/B as CNα and CNβ, respectively.

Hyperactivation of CN, due to chronic and/or exacerbated cytosolic Ca^{2+} increases, has been demonstrated to mediate L-glutamate induced hippocampal neuron death by dephosphorylating the pro-apoptotic Bcl-2-associated death promoter (BAD) (Wang et al., 1999). Indeed, multiple neurodegenerative disorders have been associated with low levels of phosphorylated BAD (Reese et al., 2008; Agostinho et al., 2008). However, the role of individual calcineurin isoforms in astrocytes is unclear.

Located between blood vessels and neurons, astrocytes make crucial contributions to the normal function of the central nervous system (CNS) (Nedergaard, 1994; Trendelenburg & Dirnagl, 2005). In addition, astrocytes respond to different kinds of CNS insults, such as infections, trauma, and ischemia by a process named reactive astrogliosis, (Kurz et al., 2005). Interestingly, CNβ was found up-regulated in reactive astrocytes of *Mongolian gerbils* after transient ischemia (Hashimoto et al., 1998); however, the functional impact of CNβ in astrocytes has not yet been determined.

Abbreviations: UPR, unfolded protein responses; CN, calcineurin; eIF2α, eukaryotic initiation factor 2 alpha; PERK, protein kinase RNA-like endoplasmic reticulum kinase; TBI, traumatic brain injury; GFAP, glial fibrillary acidic protein; Tg, thapsigargin; OGD, oxygen glucose deprivation.

* Corresponding authors at: Department of Cellular & Structural Biology, UTHSCSA, 8403 Floyd Curl Drive San Antonio, TX 78229-3904, USA; Instituto de Investigación Médica M y M Ferreyra, INIMEC-CONICET, Universidad Nacional de Córdoba, Córdoba, Argentina.
E-mail address: lechleiter@uthscsa.edu (J.D. Lechleiter).

Available online on ScienceDirect (www.sciencedirect.com).

http://dx.doi.org/10.1016/j.nbd.2016.06.011

The endoplasmic reticulum (ER) is a major signal transduction organelle essential for protein folding and assembly (Ellgaard & Helenius, 2003) as well as the regulation of intracellular Ca^{2+} stores (Brostrom & Brostrom, 2003). Transient cerebral ischemia is known to impair ER function by disturbing ER Ca^{2+} homeostasis and by depriving cells of energy (Paschen, 2004). ER stress activation during acute brain damage has also been documented after TBI (Krajewska et al., 2011; Farook et al., 2013). An immediate response to ER stress is the attenuation of protein translation *via* dimerization and autophosphorylation of protein kinase RNA-like endoplasmic reticulum kinase (PERK), which subsequently phosphorylates eukaryotic initiation factor 2 alpha (eIF2α) (Kaufman, 2004; Ma et al., 2002; Ron & Walter, 2007). The central role of ER stress and in particular, PERK, in transient cerebral ischemia is supported by an observed increase in the phosphorylation of PERK but not of other eIF2α kinases in cortex and hippocampus (Kumar et al., 2001; Kumar et al., 2003; Owen et al., 2005). We have previously shown that the PERK arm of the unfolded protein response (UPR) is activated in astrocytes within 30 min of oxygen glucose deprivation (OGD) *in vitro* (Bollo et al., 2010). However, the precise molecular mechanisms of PERK regulation in astrocytes after acute brain injury are unknown.

Contrary to previous studies that have linked exacerbated and prolonged cytosolic Ca^{2+} release to CN over-activation and neuronal death, we demonstrate here that CNβ promotes cell survival after acute brain injuries. Our evidence indicates that this is due to an interaction of CNβ with PERK, which is significantly increased by moderate cytosolic Ca^{2+} release in astrocytes during ER stress. Moreover, we demonstrate that the cytoprotective effect of CNβ is *in vivo* linked to PERK activity and correlates with reactive astrogliosis.

2. Results

2.1. CNβ, but not CNα, is significantly increased in astrocytes after traumatic brain injury

We first examined whether the CNβ isoform was up-regulated in astrocytes *in vivo* after a traumatic brain injury (TBI). TBI was induced using a controlled closed cortical impact (CCCI) model in the left parietal cortex (ipsilateral) without touching the right cortex (contralateral) (Fig. 1G) (Talley Watts et al., 2013). We observed low levels of CNβ expression that co-localized with glial fibrillary acidic protein (GFAP), considered to be expressed mainly by astrocytes (Fig. 1C). At 24 h post-TBI, the ipsilateral hippocampus showed a remarkable increase in CNβ expression in astrocytes, compared to the contralateral side or the sham group (Fig. 1A–C, H). In contrast, the same brain slices did not stain positive for CNα in astrocytes in both sides of the brain, corroborating the *in vivo* isoform cell specificity (Fig. 1D). Additionally, the expression of CNα did not change in response to TBI (Fig. 1D–F, I).

Perturbation of Ca^{2+} homeostasis has been implicated in the pathophysiology of cerebral ischemia and other brain injuries (Paschen, 2004). To recapitulate the *in vivo* situation, we used the ER Ca^{2+}-ATPase inhibitor, thapsigargin (Tg), to reduce ER Ca^{2+} stores and induce ER stress (Bollo et al., 2010; Thastrup et al., 1990). C8D1A cells (type I astrocyte cell line) were treated with 1 μM Tg for 1 h. Immunoblots showed that CNβ levels significantly increased by 2-fold as compared to dimethylsulfoxide (DMSO, Con) treatment (Supplementary Fig. 1A, B). However, the levels of the α isoform of CN remained unchanged (Supplementary Fig. 1A, B). We also determined CN expression after OGD. Again, CNβ levels were significantly increased in mouse primary astrocytes after 30 min (Supplementary Fig. 1C, D), suggesting a role for CNβ under conditions of astrocyte acute stress.

2.2. CNβ null mice exhibit higher lesion volume and increased cytotoxic edema after TBI

To further determine the potential role of CNβ in acute brain injury, we compared the outcome of CCCI induced TBI on CNβ wildtype ($\beta^{+/+}$) and knockout ($\beta^{-/-}$) mice. Lack of CNβ protein in null mice was confirmed by immunoblotting (Klee et al., 1998). CNα expression was clearly detected in mice of both genotypes (Fig. 2B) (Wu et al., 2004). At 24 h post-TBI, Nissl staining showed significantly increased lesion volume in $\beta^{-/-}$ mice by over 2-fold compared with lesion volume in $\beta^{+/+}$ mice (Fig. 2A, C). $\beta^{-/-}$ mice also demonstrated a remarkable increase in the soma size of neurons in both the ipsilateral cortex and hippocampal CA1 region as compared to $\beta^{+/+}$ mice (Fig. 2D–G). Together, these data suggest that loss of CNβ significantly worsens the outcome of acute brain injury.

2.3. CNβ physically interacts with PERK and promotes PERK oligomerization and phosphorylation in stressed astrocytes

We show here that conditions that upregulated CNβ in C8D1A astrocytes (Supplementary Fig. 1) also increased the levels of phosphorylated PERK (P-PERK) and eIF2α (P-eIF2α) (Fig. 3A, B) (Mounir et al., 2011). Protein lysates from C8D1A cells exposed to 1 μM Tg for 1 h and probed for PERK and eIF2α on immunoblots were found to have significantly increased expression of the phosphorylated forms of PERK and eIF2α (Fig. 3 A, B). Immunostaining also demonstrated increased P-PERK in astrocytes exposed to Tg (Supplementary Fig. 2A–C). Consistently, OGD also increased P-PERK expression in primary mouse astrocytes (Supplementary Fig. 2D–F). Taken together, our results indicate that induction of CNβ is correlated with phosphorylation of PERK and eIF2α in astrocytes in conditions that mimic ischemic stress *in vivo*.

The association of the α isoform of CN (CNα) and PERK under acute ER stress has been studied in *Xenopus* oocytes, but CNβ was not detected in these cells (Bollo et al., 2010). Both our *in vitro* and *in vivo* data suggest that CNβ is the major isoform of CN in stressed astrocytes. Given that P-PERK was enhanced in astrocytes during ER stress, we hypothesized that CNβ directly interacted with PERK to modulate cell stress that occurs after brain injury (Nakka et al., 2014). To test this hypothesis, we examined whether endogenous CNβ interacted with endogenous PERK in stressed primary astrocytes by co-immunoprecipitation. As shown in Fig. 3 (C, D), increased P-PERK was bound to CNβ on treatment of primary astrocytes with Tg. Next, we performed pull-down assays using purified recombinant GST-cytosolic PERK (GST-cPERK) and either His-CNα or His-CNβ (Fig. 3E, F). We note that all of the pull-down assays were performed using the same stringency conditions (high ionic strength and in the presence of detergent). These experiments revealed that the association between CNβ and GST-cPERK was significantly weaker than the CNα/PERK interaction. Finally, we performed an *in vitro* kinase assay to determine the functional consequences of these interactions. To do this, the same recombinant proteins were incubated with [γ^{32}P] ATP (Fig. 3G, H). We found that the β isoform was able to promote PERK autophosphorylation at a level significantly higher than the α isoform. These data demonstrate that the efficacy for promoting PERK phosphorylation did not necessarily depend on the strength of interaction.

We also investigated the potential effect of the CN regulatory subunit (CN-B) on PERK interaction and auto-phosphorylation (Supplementary Fig. 3). However, in order to detect a trend in specific interaction with GST-cPERK compared with GST only (negative control; Supplementary Fig. 3A, B), we required a 1000-fold higher concentration of CN-B compared to the association with the heterodimer (subunits A and B, Fig. 3E, F). Interestingly, CN-B was unable to promote GST-cPERK auto-phosphorylation even when added at a concentration higher than the heterodimer (Supplementary Fig. 3C, D).

Overall, these data demonstrate that direct interaction of CNβ/PERK promotes PERK phosphorylation in astrocytes during acute ER stress. It has been proposed that formation of PERK oligomers is a step that precedes trans-autophosphorylation (Polley et al., 2013; Bertolotti et al., 2000) Therefore, we tested if CNβ promotes PERK cluster formation or alternatively if CNβ interacts with PERK after PERK has oligomerized. We incubated GST-cPERK with increased concentrations of CNβ and a crosslinker, disuccinimidyl suberate (DSS). The complex was run on a

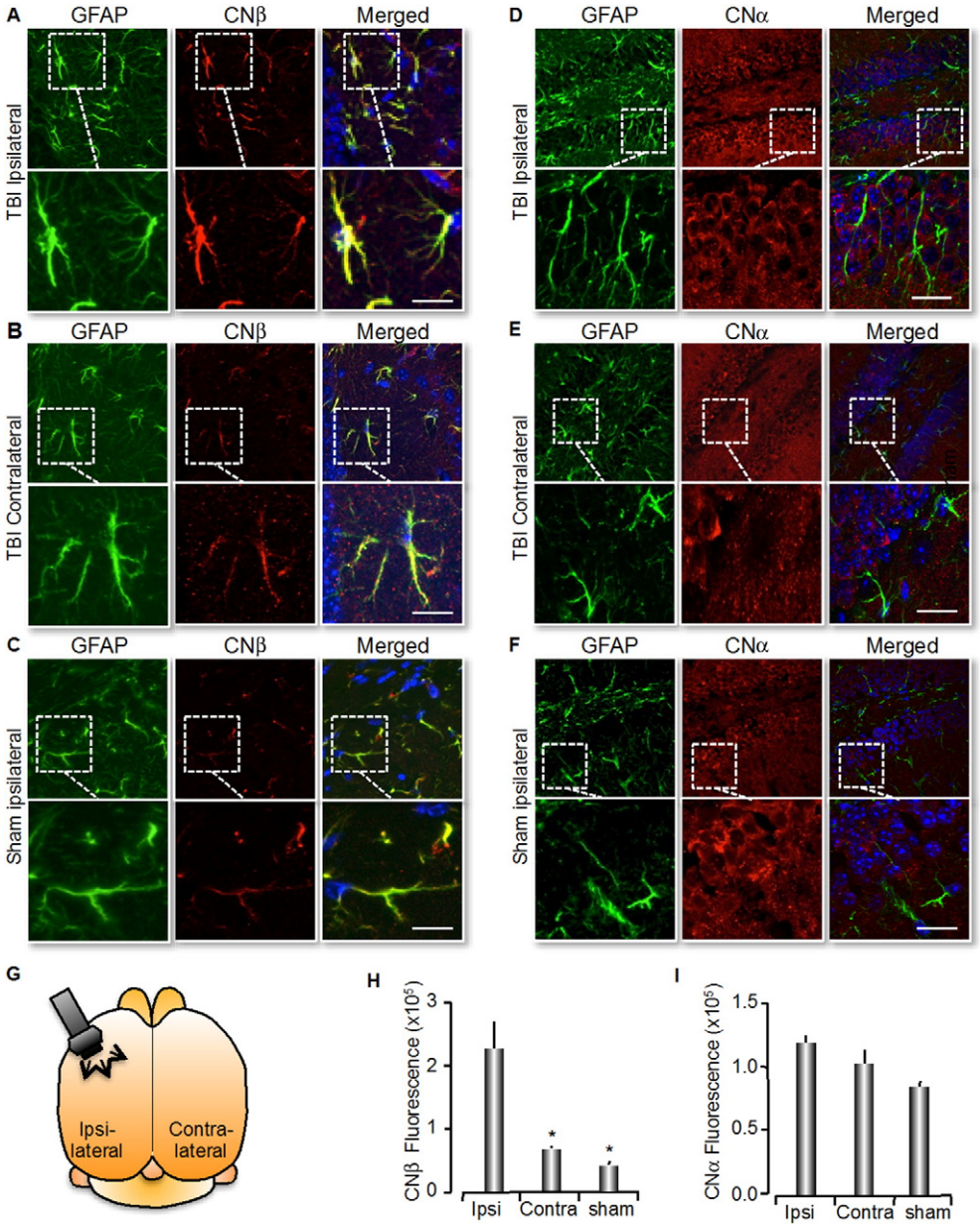

Fig. 1. CNβ, but not CNα, expression increases in astrocytes *in vivo* after TBI. Representative Z-projection merged images of mice brains harvested 24 h post-TBI and stained with antibodies against CNβ or CNα (red), GFAP (green) and DAPI (nuclei, blue). Images were acquired on an Olympus FV1000 confocal microscope. (A, D) Ipsilateral side of TBI brain sections; (B, E) Contralateral side of TBI brain sections; (C, F) Brain sections from sham mice. (G) Schematic diagram of brain undergoing TBI. Ipsilateral and contralateral sides of trauma are labeled. (H, I) Quantification of fluorescence intensity in panels above from 3 mice ($n = 3$, mean ± SEM, $^*p < 0.05$ by one-way ANOVA). Scale bar: 10 μm (A-C); 20 μm (D–F).

gel under reducing conditions and probed with an anti-PERK antibody (Fig. 3I). In solution, GST-cPERK existed not only as monomers but also as stable dimers and oligomers. This was likely due to dimerization of the GST portion of GST-cPERK as reported by several groups (Parker et al., 1990; Ji et al., 1992; Welihinda & Kaufman, 1996) and also due to the presence of a dimerization subdomain located in the cytosolic domain of PERK (Yamani et al., 2014). We observed that increasing concentrations of CNβ resulted in more dimers and oligomers of GST-cPERK. The same crosslinking assay was performed on purified CNβ and maltose binding protein (MBP)-cPERK, in which MBP is fused with His-cPERK to increase protein solubility. Similar to GST, MBP portions dimerized by themselves as reported previously (Richarme, 1982). As with GST-cPERK, we also observed increased dimers and oligomers of MBP-cPERK with increasing concentration of CNβ (Supplementary Fig. 3E). We note that the difference in the molecular weight of the PERK monomers is due to the fusion tags to the proteins (~25 KDa and 42 KDa for GST and MBP, respectively). In another set of experiments, we cross-linked GST-cPERK with 1.2 μM of CNβ. Immunodetection using anti-CNβ and anti-PERK antibodies confirmed increased level of high molecular weight CN concurrently with the oligomerization of GST-cPERK and that the presence of CN induced PERK oligomerization (Fig. 3J). We note that the phosphorylated form of PERK is expected to run as a heterogeneous population (smear), because of the many phosphorylation sites in the PERK protein (Volmer et al., 2013). Therefore, CNβ participates in PERK cluster formation and we conclude that CNβ acts as a cytosolic ligand to promote PERK oligomerization, favoring PERK trans-autophosphorylation and its kinase activity.

. (D) Quantification of P-PERK/T-PERK densitometric ratio in (C) ($n = 3$, mean ± SEM, $^*p < 0.05$ by unpaired two-tailed Student's *t*-test). (E) GST *pull-down* assay with either 8 nM of CNα or CNβ. The proteins were incubated with glutathione sepharose 4B for 1 h, resolved on a 12% SDS-polyacrylamide gel and probed with an anti-calcineurin PAN-

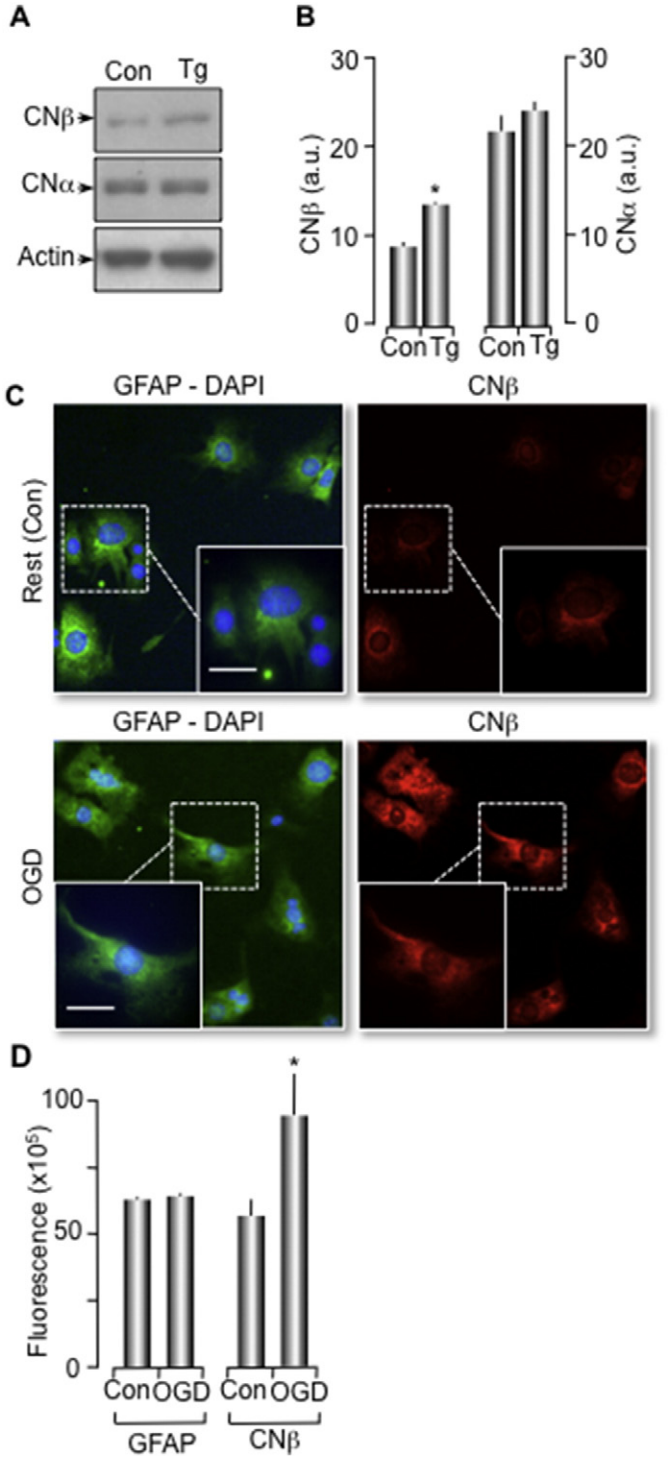

Supplementary Fig. 1. CNβ, but not CNα, is upregulated during stress in astrocytes *in vitro*. (A) C8D1A type I astrocytes were treated with vehicle (DMSO; Con) or 1 μM of thapsigargin (Tg) for 1 h. Cell lysates were analyzed for CNβ and CNα expression by immunoblotting. (B) Densitometry histograms after normalization to actin (n = 3, mean ± SEM, $^{*}p < 0.05$ by unpaired two-tailed Student's *t*-test). (C) Cultured mouse primary astrocytes were exposed to oxygen glucose deprivation (OGD) for 30 min, fixed and immunostained for CNβ (red), GFAP (green) and DAPI (nuclei, blue). Images were sequentially acquired on a Nikon TE300 microscope. Scale bar: 20 μm. (D) Fluorescence intensities in (C) from three different independent experiments in which at least 10 cells were quantified per experiment (n = 3, mean ± SEM, $^{*}p < 0.05$ by unpaired 2-tailed Student's *t*-test).

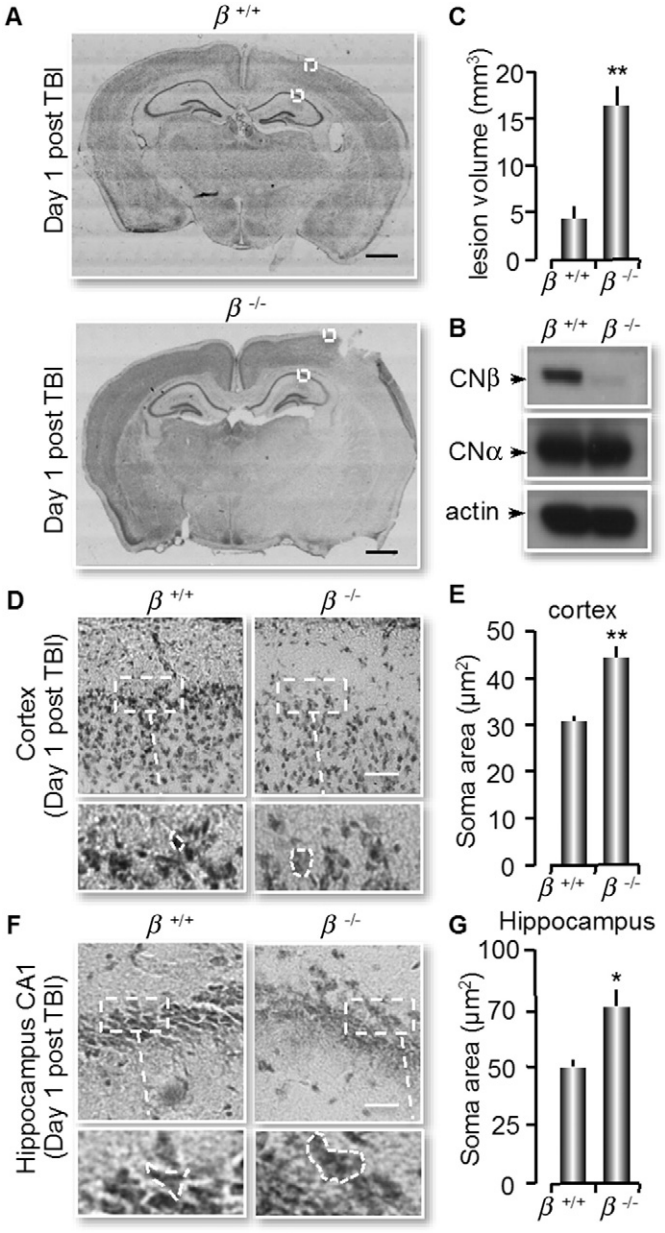

Fig. 2. CNβ null mice exhibit higher lesion volume and increased cytotoxic edema in neurons after TBI. (A) Nissl staining of coronal sections from CNβ wildtype ($\beta^{+/+}$) and null ($\beta^{-/-}$) mice 24 h post-TBI. Dashed boxes represent areas shown in D and F, respectively. Scale bar: 1 μm. (B) Immunoblots of homogenized brain lysates from $\beta^{+/+}$ and $\beta^{-/-}$ mice for CNα and CNβ. Actin was used as a loading control. (C) Quantification of lesion volume by Nissl staining shown in (A) (n = 3, mean ± SEM, $^{*}p < 0.05$, by unpaired two-tailed Student's *t*-test). (D, F) Higher magnification images from the cortex and the CA1 region of the hippocampus from $\beta^{+/+}$ and $\beta^{-/-}$ mice. Scale bar: 10 μm. (E, G) Quantification of averaged neuron soma size in the cortex and the CA1 region of the hippocampus after TBI, respectively (n = 3, mean ± SEM, $^{*}p < 0.05$, $^{**}p < 0.01$ by unpaired two-tailed Student's *t*-test).

A antibody. CN *pull-down* levels are shown for GST alone and GST-cPERK. (F) Densitometric histogram of (E) (n = 3, mean ± SEM, $^{**}p < 0.01$ by unpaired two-tailed Student's *t*-test). (G) GST-cPERK was added to all reaction mixtures along with [γ^{32}P] ATP in the absence or the presence of either of 0.043 μM of CNα or CNβ. Reaction mixtures were run on SDS-PAGE and visualized by autoradiography. (H) Quantification of cPERK auto-phosphorylation density (n = 5, mean ± SEM, $^{*}p < 0.05$ by one-way ANOVA). (I) Recombinant His-CNβ and GST-cPERK were incubated at the concentrations indicated, in the presence of 0.3 mM of DSS cross-linker for 30 min at room temperature. The ensuing protein complexes were run on SDS-PAGE and detected by immunoblotting using an anti-PERK antibody. (J) Recombinant His-CNβ (1.2 μM) and GST-cPERK (0.01 μM) were incubated in the presence of

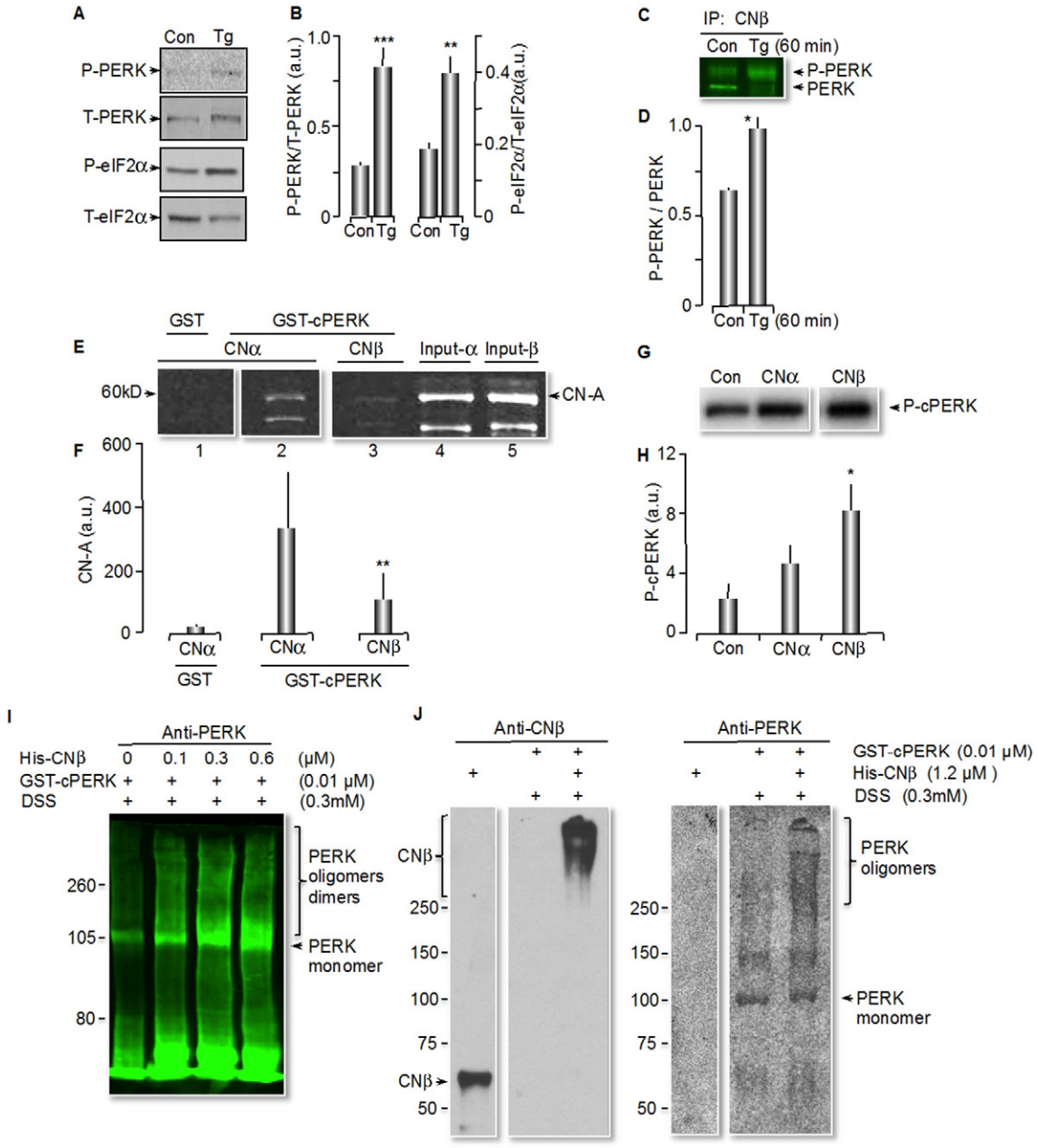

Fig. 3. CNβ physically interacts with PERK and promotes PERK phosphorylation and oligomerization. (A) C8D1A type I astrocytes were treated with vehicle (DMSO; Con) or 1 μM of thapsigargin (Tg) for 1 h. Cell lysates were analyzed for total (T) and phosphorylated (P) PERK and eIF2α using immunoblots. (B) Densitometry histograms after normalization to T-PERK or T-eIF2α, respectively (n = 3, mean ± SEM, $^{**}p < 0.01$ and $^{***}p < 0.001$ by unpaired two-tailed Student's *t*-test). (C) Primary mouse astrocytes were treated as indicated in (A) and then cross-linked with disuccinimidyl suberate (DSS) for 30 min. Immunoprecipitation (IP) was performed with anti-CNβ antibody and subsequent blots were probed with anti-PERK antibody. (D) Quantification of P-PERK/T-PERK densitometric ratio in (C) (n = 3, mean ± SEM, $^{*}p < 0.05$ by unpaired two-tailed Student's *t* test). (E) GST *pull-down* assay with either 8 nM of CNα or CNβ. The proteins were incubated with glutathione sepharose 4B for 1 h, resolved on a 12% SDS-polyacrylamide gel and probed with an anti-calcineurin PAN-A antibody. CN *pull-down* levels are shown for GST alone and GST-cPERK. (F) Densitometric histogram of (E) (n = 3, mean ± SEM, $^{**}p < 0.01$ by unpaired two-tailed Student's *t* test). (G) GST-cPERK was added to all reaction mixtures along with [g^{32}P] ATP in the absence or the presence of either of 0.043 mM of CNα or CNβ. Reaction mixtures were run on SDS-PAGE and visualized by autoradiography. (H) Quantification of cPERK auto-phosphorylation density (ne = 5, mean ± SEM, $^{*}p < 0.05$ by one-way ANOVA). (I) Recombinant His-CNβ and GST-cPERK were incubated at the concentrations indicated, in the presence of 0.3 mM of DSS cross-linker for 30 min at room temperature. The ensuing protein complexes were run on SDS-PAGE and detected by immunoblotting using an anti-PERK antibody. (J) Recombinant His-CNβ (1.2 mM) and GST-cPERK (0.01 mM) were incubated in the presence of 0.3 mM of DSS for 30 min at room temperature. The protein complexes were run on SDS-PAGE and detected by immunoblotting using antibodies against CNβ and PERK.

0.3 mM of DSS for 30 min at room temperature. The protein complexes were run on SDS-PAGE and detected by immunoblotting using antibodies against CNβ and PERK.

2.4. Chemical or light induced-dimerization induces immediate CNβ/PERK interaction in live cells, resulting in PERK phosphorylation

To determine if the observed CNβ and PERK interaction *in vitro* also occurred in live cells, we took advantage of the rapamycin-driven heterodimerization technique (Komatsu et al., 2010) to confirm the effect of acute CN-PERK interaction in live cells (Komatsu et al., 2010). This module was based on the rapamycin-induced FK506 binding protein (FKBP)/FKBP-rapamycin binding domain (FRB) interaction. For these experiments, the effector (FKBP-YFP-CNβ) and anchor (FRB-CFP-Cb5) units were overexpressed in human astrocytes. The anchor unit has the transmembrane domain of cytochrome b5, an ER membrane protein, tail-anchored to the cytoplasmic face of the ER (Supplementary Fig. 4A) (Honsho et al., 1998); thus, we were able to observe the ER structure

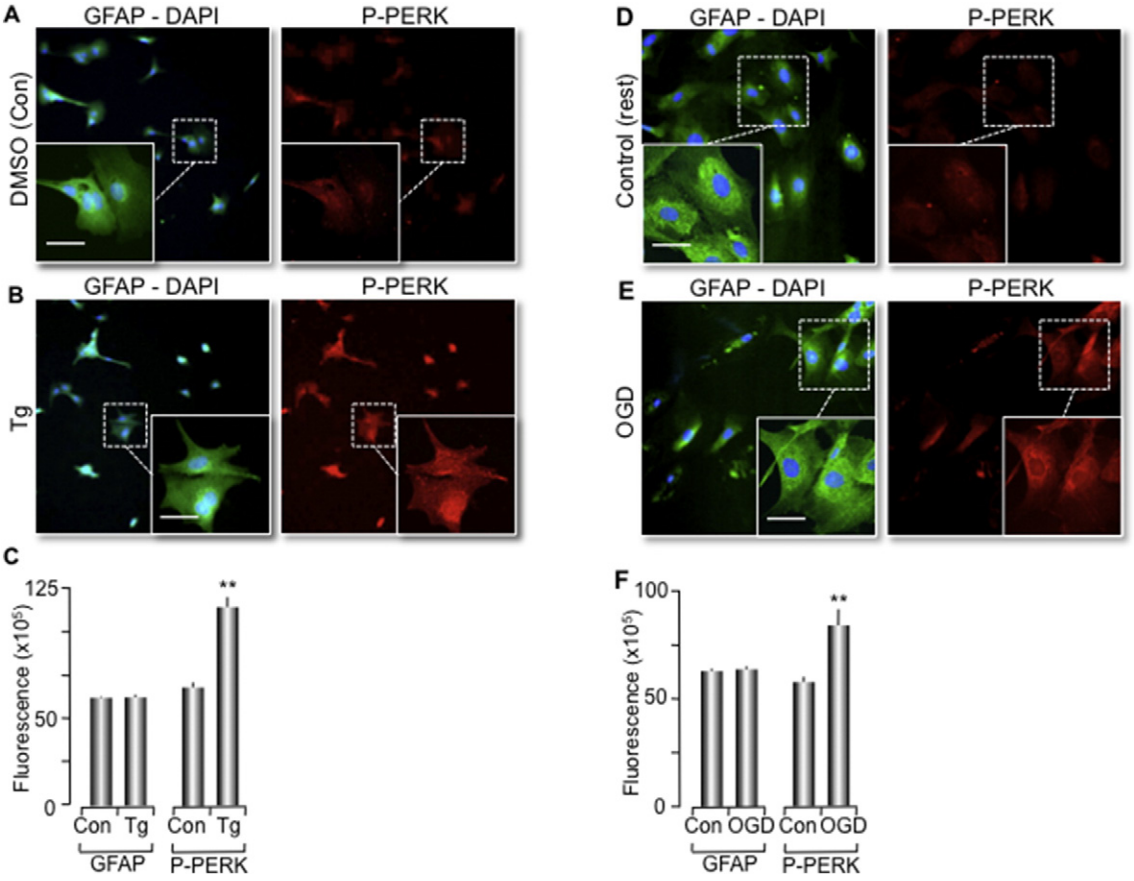

Supplementary Fig. 2. ER stress induces PERK phosphorylation in cultured astrocytes. (A, B) C8D1A cells were exposed to Tg for 1 h fixed and immunostained for P-PERK (red), GFAP (green) and DAPI (nuclei, blue). Images were sequentially acquired on a Nikon TE300 microscope. Scale bar: 20 μm. (C) Mean fluorescence intensities in (A, B) from three independent experiments in which at least 10 cells were quantified per experiment (mean ± SEM, $^{**}p < 0.01$, by unpaired two-tailed Student's *t*-test). (D, E) Cultured mouse primary astrocytes were exposed to OGD for 30 min, fixed, immunostained and images acquired as (A, B). Scale bar: 20 μm. (F) Mean fluorescence intensities in (D, E) from three independent experiments in which at least 10 cells were quantified per experiment (mean ± SEM, $^{**}p < 0.01$ by unpaired two-tailed Student's *t*-test).

with CFP and cytosolic distribution of YFP (Fig. 4E, H). After addition of 100 nM rapamycin, FKBP-YFP-CNβ was recruited to the ER, where FRB-CFP-Cb5 was located (Fig. 4C). Immunostaining showed that cells with CNβ translocation exhibited a significant increase in P-PERK fluorescence intensity (Fig. 4D, K). However, in DMSO (vehicle)-treated cells, neither translocation of CNβ nor changes in P-PERK was observed (Fig. 4A, B, K). Together, these data reveal that recruitment of CNβ to the ER membrane in live cells facilitates CNβ-PERK interaction and leads to PERK autophosphorylation.

Previous studies have shown that intracellular Ca^{2+} levels can affect PERK and CN dynamics (Bollo et al., 2010; Wang et al., 2013). Therefore, we tested the effect of intracellular Ca^{2+} levels on CN-mediated PERK activation. We added a very low concentration of Tg to induce Ca^{2+} release (Supplementary Fig. 4B) (Kovacs et al., 2005). DMSO with Tg caused neither the translocation of CNβ in YFP nor significant changes in P-PERK intensity (Fig. 4F, G, K), suggesting that at low concentration of Tg, the moderate cytosolic Ca^{2+} increase is not sufficient to have effect on PERK phosphorylation by itself. However, cells with both rapamycin and Tg treatment showed co-localization of YFP-CNβ with the CFP-ER anchor. These cells also displayed increased P-PERK compared with non-transfected neighbor cells (Fig. 4I—K). P-PERK intensity was increased by 30% in cells that received both rapamycin and Tg, compared with the rapamycin-only treatment group (Fig. 4K). These results are consistent with previous data from our group (Bollo et al., 2010; Paredes et al., 2013) and indicate that Ca^{2+} release from ER enhances PERK activation.

2.5. CNβ induces PERK phosphorylation independent of its phosphatase activity

To determine if the enzymatic activity of CNβ was required or altered in mediating its effects on PERK phosphorylation, we constructed a pUltra-lentiviral vector to overexpress CNβ in cultured astrocytes. Immunoblots showed a 2-fold increase in the levels of CNβ in lenti-GFP (CNβ) transduced astrocytes and correspondingly, increased P-PERK levels compared with lenti-GFP (control) transduced cells (Supplementary Fig. 5). Similar to the results from western blots, an immunocytochemistry assay showed that CNβ levels were increased in cultured astrocytes infected with lentivirus lenti-GFP (CNβ) compared to those infected with lenti-GFP (Fig. 5A, B, G). The levels of P-PERK were increased by over 5-fold in the astrocytes that overexpressed CNβ (Fig. 5C, D, H). Next, we exposed these astrocytes to quercetin (QC), a novel non-competitive CN inhibitor with strong phosphatase inhibitory activity (Wang et al., 2010; Lei et al., 2011). Interestingly, the presence of the CN inhibitor did not interfere with PERK phosphorylation in cells overexpressing CNβ ($n = 3$, $^{***}p < 0.001$) (Fig. 5E, F, H). These data strongly suggest that the effect of CNβ on PERK phosphorylation is independent of its phosphatase activity.

2.6. PERK is required for CNβ-mediated protection of astrocytes

We also investigated the physiological consequences of increased expression of CNβ in ER-stressed astrocytes from both PERK null mice

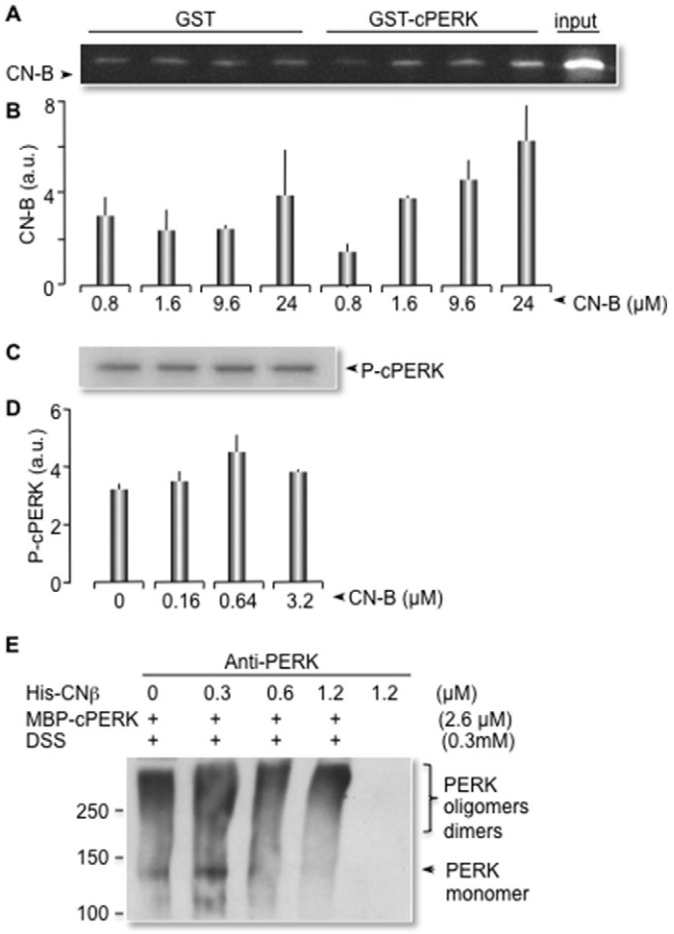

Supplementary Fig. 3. Regulatory subunit B does not promote PERK autophosphorylation, but the heterodimer of CNβ promotes PERK dimerization and oligomerization. (A) GST *pull-down* assay using His-CN-B and GST-cPERK. The proteins were incubated at concentrations indicated with glutathione sepharose 4B and resolved on a 12% SDS-polyacrylamide gel and probed using an anti-CN-B mouse monoclonal antibody. (B) Densitometric histogram based on an average of three independent experiments (mean ± SEM, one-way ANOVA). (C) GST-cPERK and His-CN-B were incubated with [γ^{32}P] ATP (5500 Ci. pmols^{-1}), resolved through 10% SDS-PAGE and visualized by autoradiography. Phosphorylation levels are shown for GST-cPERK in the absence or the present of CN-B at indicated concentrations. (D) Densitometric histogram of GST-cPERK phosphorylation based on the average of three independent experiments (mean ± SEM, one-way ANOVA). (E) Recombinant proteins His-CNβ (the heterodimer) and maltose binding protein (MBP)-cPERK were incubated at the indicated concentrations, in the presence of 0.3 mM of DSS cross-linker for 30 min at room temperature. The protein complexes were run on SDS-PAGE and detected by immunoblotting with the anti-PERK antibody.

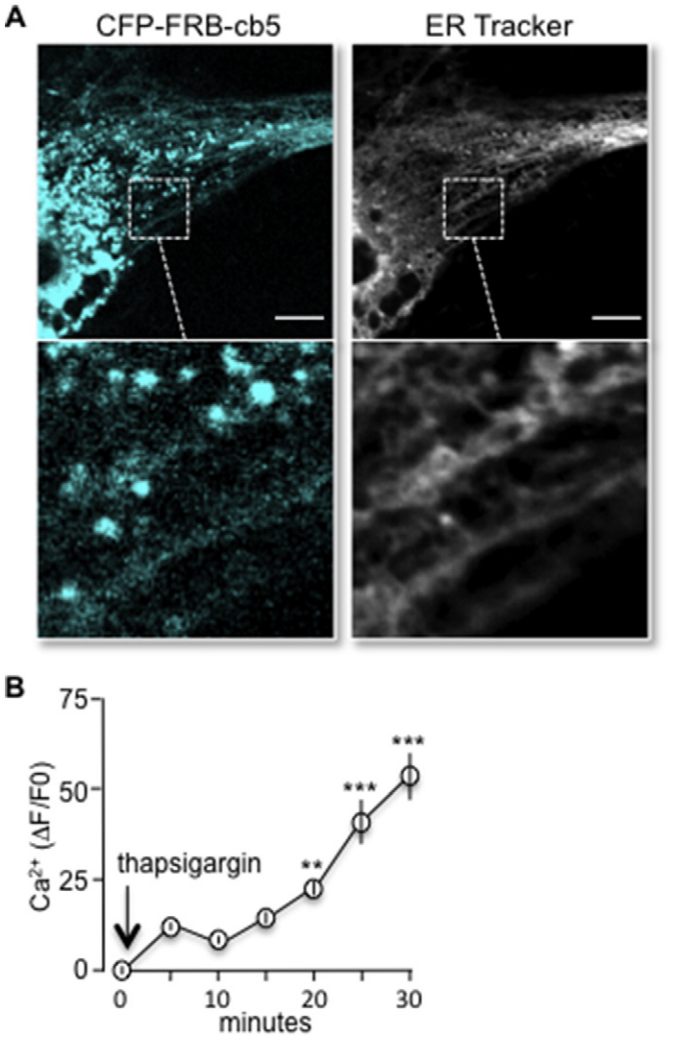

Supplementary Fig. 4. CFP-FRB-cb5 localizes to the ER; Tg evokes significant Ca^{2+} release within 20 min. (A) CFP-FRB-cb5 localizes to the ER. Human astrocytes expressing CFP-FRB-cb5 were incubated with the ER-tracker dye (blue-white DPX) for 30 min. Confocal images were acquired on an Olympus FV1000 confocal microscope. Scale bar: 10 μm. (B) Tg at low concentrations can evoke significant calcium (Ca^{2+}) release in 20 min. Cultured human astrocytes were loaded with Fluo-4 AM and treated with 25 nM of Tg. Images were acquired at the distinct time points on a Nikon swept field confocal microscope. ΔF/F0 is the ratio of changes in mean fluorescence intensities to the baseline intensity of Fluo-4 (n = 3, mean ± SEM, $^{**}p < 0.01$, $^{***}p < 0.001$ by one-way ANOVA).

($Perk^{-/-}$) and wild type siblings ($Perk^{+/+}$). CN overexpression by lentiviral infection did not cause significant changes in cell viability of $Perk^{+/+}$ and $Perk^{-/-}$ astrocytes at rest (Fig. 6A, C, F, H; Supplementary Fig. 6A–C). Treatment of pUltra lentivirus transduced cells with *tert*-butyl hydroperoxide (tBuOOH) (He et al., 2008) for 2 h or OGD for 1 h showed that overexpression of CNβ increased the percentage of live cells from 42% to 51% (Fig. 6A, B, E) and from 50% to 69% (Fig. 6F, G, J), respectively. However, overexpression of CNβ in $Perk^{-/-}$ astrocytes had no significant effect on cell survival (Fig. 6C–E, H–J). These findings strongly indicate that lack of PERK abolishes the protective effect of CNβ on stressed astrocytes.

In a similar experiment, we overexpressed CNβ in astrocytes using transient transfection and exposed these cells to tBuOOH for 2 h. We observed 50% cell death in untransfected cells (Con) whereas overexpression of CNβ reduced cell death by 25% (n = 4, $^{**}p < 0.01$) (Supplementary Fig. 6D, E). More interestingly, there was no significant difference in viability of Perk-deficient cells with overexpression of CNβ as compared to control cells.

2.7. PERK is required for CNβ-mediated protection from brain injury in vivo

To determine the involvement of PERK in CNβ-mediated protection from acute brain injury, we measured the ischemic outcome of mice with pharmacologically inhibited PERK activity. GSK2656157 is a potent and selective inhibitor of PERK kinase (Axten et al., 2012). We injected GSK2656157 intraperitoneally into wildtype ($\beta^{+/+}$) mice. Immunoblots of brain tissue showed that P-PERK and P-eIF2α were significantly inhibited at 12 h after administration of PERK inhibitor (Fig. 7A, B). At this time point, we induced a photothrombotic stroke in mice using Rose-Bengal (RB) dye (Fig. 7C). Fluorescence gradually disappeared in the target vessel, suggesting that a stable clot was formed (Fig. 7C). After 24 h, brain slices were stained with the vital dye, 2,3,5-triphenyltetrazolium chloride (TTC) (Fig. 7D). The absence of staining indicated necrotic tissue and this was used to define the area of brain infarction.

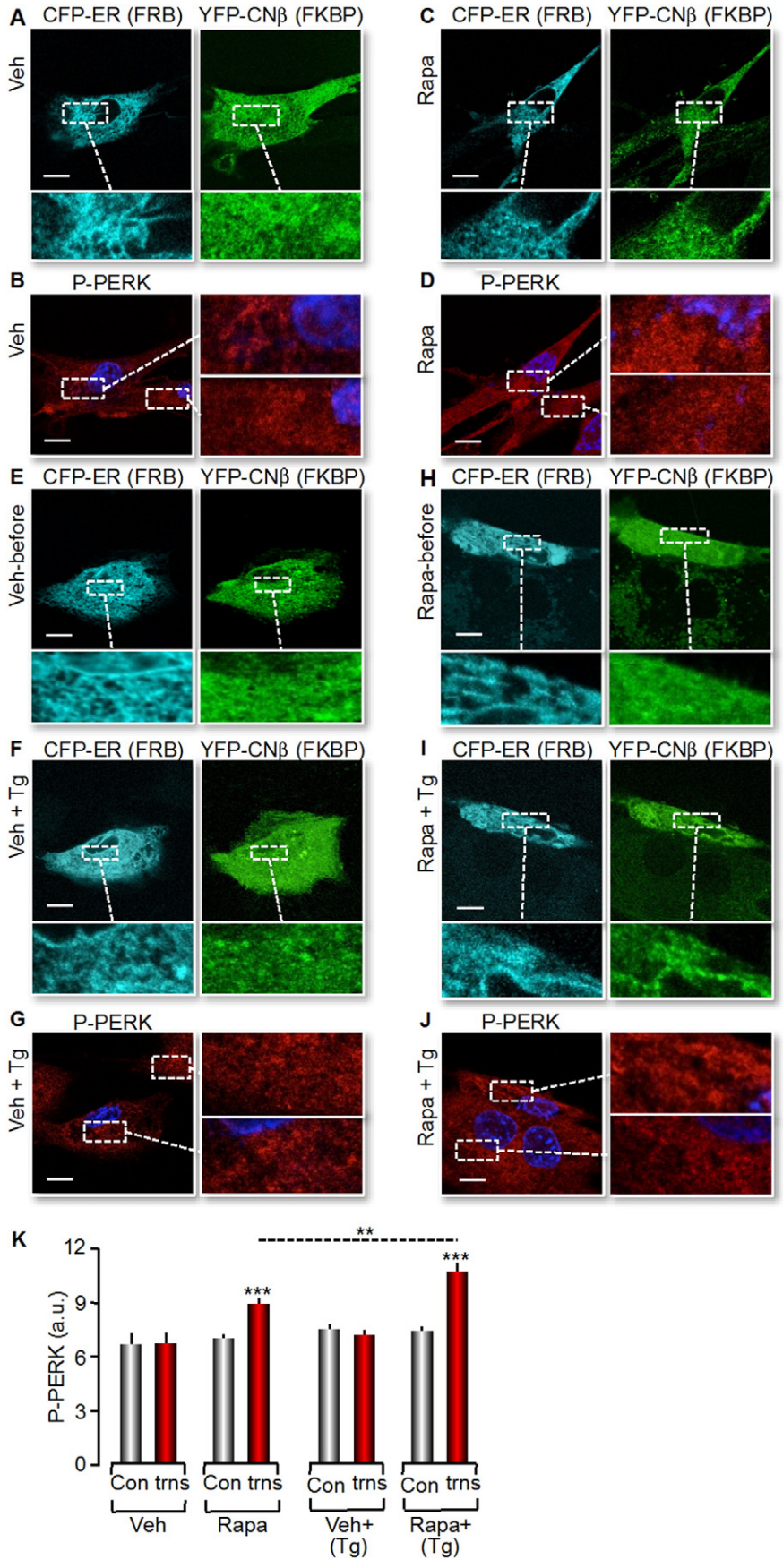
A
CFP-ER (FRB)
YFP-CNβ (FKBP)
Veh
C
CFP-ER (FRB)
YFP-CNβ (FKBP)
Rapa
B
P-PERK
Veh
D
P-PERK
Rapa
E
CFP-ER (FRB)
YFP-CNβ (FKBP)
Veh-before
H
CFP-ER (FRB)
YFP-CNβ (FKBP)
Rapa-before
F
CFP-ER (FRB)
YFP-CNβ (FKBP)
Veh + Tg
I
CFP-ER (FRB)
YFP-CNβ (FKBP)
Rapa + Tg
G
P-PERK
Veh + Tg
J
P-PERK
Rapa + Tg
K
**
***
***
P-PERK (a.u.)
12
9
6
3
0
Con trns
Con trns
Con trns
Con trns
Veh
Rapa
Veh+ (Tg)
Rapa+ (Tg)

The average infarct volume in $\beta^{+/+}$ mice was 3.61 ± 0.88 mm^3. This volume was significantly increased by two-fold when PERK activity was inhibited (Fig. 7E).

To investigate the role of PERK-CNβ interaction after brain ischemia, we first measured cerebral damage in $\beta^{-/-}$ mice after acute stroke. This average infarct volume in $\beta^{-/-}$ mice was 10.54 ± 2.11 (n = 5) mm^3, which is significantly larger than that in $\beta^{+/+}$ mice (Fig. 7D, E). Importantly, administration of PI did not change the infarct size in mice deficient in $\beta^{-/-}$ mice (Fig. 7D, E).

In parallel, we directly injected the PI into the lateral ventricle, as illustrated by Evans blue staining (Supplementary Fig. 7A). Significant decreases in P-PERK and P-eIF2α levels were observed at 12 h after micro-injection of PI (Supplementary Fig. 7 B, C). RB-induced photothrombosis was performed on the contralateral side of micro-injection (Supplementary Fig. 7D), resulting in a doubled stroke volume in PI-treated group compared to Con group (Supplementary Fig. 7E, F). Taken together, these data strongly suggest that PERK activity is important for protection following acute cerebral ischemia and that CNβ and PERK might function through the same cytoprotective pathway after ischemia.

Related to these data we also discovered that in $\beta^{+/+}$ mice, GFAP expression and the size of astrocytes near the infarct were significantly increased in the ipsilateral side of stroke as compared to the contralateral side, indicating increased proliferation of reactive astrocytes (Stichel & Muller, 1998) (Fig. 8A, B, G). We also noticed a significant increase in phosphorylation of eIF2α after stroke in the ipsilateral sides in $\beta^{+/+}$ mice as compared to contralateral sides, strongly suggesting activation of the CNβ — PERK pathway (Fig. 8C, H). However, compared to $\beta^{+/+}$ mice, $\beta^{-/-}$ mice exhibited much lower levels of GFAP and P-eIF2α in reactive astrocytes as well as considerably smaller astrocytes after stroke (Fig. 8G–J). We note that GFAP expression was still significantly increased after stroke in the ipsilateral sides of $\beta^{-/-}$ mice, while P-eIF2α levels and astrocytes size were not increased when compared to the contralateral sides (Fig. 8E, F, G, H). These data indicate that up-regulation of CNβ protected against ischemic insult by enhancing PERK signaling in astrocytes, which is associated with increased overexpression of GFAP and the astrocytes size, both characteristic of reactive gliosis.

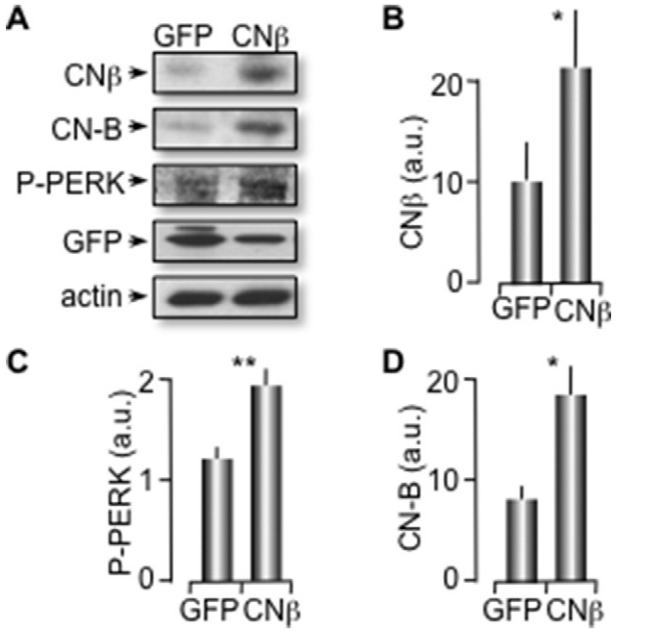

Supplementary Fig. 5. Lentivirus overexpressing CNβ and CN-B in astrocytes increases PERK phosphorylation. (A) Immunoblots probed for P-PERK, CNβ and CN-B in astrocytes infected with pUltra Lenti-GFP or Lenti-GFP (CNβ) lentivirus. GFP and actin were used as loading controls. (B-D) Quantification of the experiments in (A) (n = 3, mean ± SE, $^*p < 0.05$, $^{**}p < 0.01$ by unpaired two-tailed Student's *t*-test).

3. Discussion

In this study, we identify an unexpected protective role for CNβ in astrocytes *in vivo* using two acute brain injuries models: TBI and stroke. We show that CNβ directly interacts with PERK, promoting its dimerization/oligomerization and auto-phosphorylation, and that Ca^{2+} appears to function as a co-factor. Importantly, we demonstrate for the first time, a critical role for the β isoform of CN in cell survival after brain injury, an observation that contrasts with the established role of CN in neuronal cell death (Shioda & Fukunaga, 2011). Moreover, we show that the protective effect of CNβ appears independent from its known phosphatase activity. Finally, our data show that activation of the CN-PERK-eIF2α pathway correlates with GFAP expression, suggesting this pathway may also directly regulate reactive gliosis signaling.

Our finding that CNβ levels are increased in reactive astrocytes in the TBI mouse model is consistent with a previous report showing that CNβ was up-regulated in reactive astrocytes in ischemic hippocampal regions of Mongolian gerbils (Hashimoto et al., 1998). In contrast, it has also been reported that CN levels do not change after trauma (Kurz et al., 2005). These differences may be due to the fact that these authors used only western blots to measure CN levels and that the antibody used did not distinguish between CN isoforms. Given that CNα is more abundant than CNβ in mammalian brain (Kuno et al., 1992), we speculate that the whole brain homogenate analysis may have obscured smaller, astrocyte-specific changes in CNβ.

More importantly, our results also revealed that acute brain injury caused more damage in mice lacking CNβ. This is in agreement with our *in vitro* data showing a protective benefit of overexpressing CNβ in astrocytes. The cell survival role of CNβ in astrocytes is in contrast to the apoptotic role of CN when over-activated by chronic and exacerbated cytosolic Ca^{2+} increase in hippocampal neurons (Wang et al., 1999). This cytoprotective function also appears to be distinct from another reported role of CN in reactive astrocytes, where CN significantly diminishes inflammatory injury by its phosphatase activity and subsequent signaling of NFAT (nuclear factor of activated T) cells (Fernandez et al., 2007; Pyrzynska et al., 2001). This conclusion is based on our observation that CNβ promoted PERK phosphorylation in the presence of a phosphatase inhibitor.

In vitro experiments using recombinant proteins revealed that CNβ binds to the cytosolic domain of PERK with lower affinity than CNα, however, CNβ results in markedly higher PERK auto-phosphorylation. The regulatory subunit B of CN is unable to promote PERK auto-phosphorylation. This observation, as well as the difference in PERK binding affinity of the CN isoforms, argue against non-specific effects. Moreover, direct binding of CNβ to the higher oligomers of GST-cPERK suggests that CNβ drives PERK clustering, phosphorylation, and activation of its kinase activity. Signaling outputs from another ER stress sensor, IRE1α, have been reported to vary with its oligomerization state (Han et al., 2009). In a similar fashion, CNβ may act as a cytosolic regulator of PERK activity that helps tone the intensity of stress stimuli by modulating PERK oligomerization.

Fig. 4. Rapamycin induces CNβ translocation to ER membrane and thereby promotes PERK phosphorylation. (A, C) Confocal images of human astrocytes expressing CFP-FRB-cytochrome 5 (cb5, ER anchor) and YFP-FKBP-CNβ after addition of 100 nM of rapamycin (Rapa) for 30 min that induced translocation of the CNβ construct to the ER. DMSO-treated cells were used as controls (Veh). (*E*-F, H–I) Confocal images of cells before and after addition of 100 nM of rapa for the first 10 min and then 25 nM Tg for an additional 20 min. DMSO and Tg treatments were used as controls (Veh + Tg). (B, D, G, J) Immunocyto-chemistry was immediately performed to detect P-PERK (red). Nuclei were stained with DAPI (blue) in cells. Scale bar: 20 μm. (K) Quantification of fluorescence intensity of P-PERK in untransfected (Con) and transfected cells (trns) in (B, D, G, J) (n > 20 cells per group, mean ± SEM, $^{**}p < 0.01$, $^{***}p < 0.001$ by one-way ANOVA).

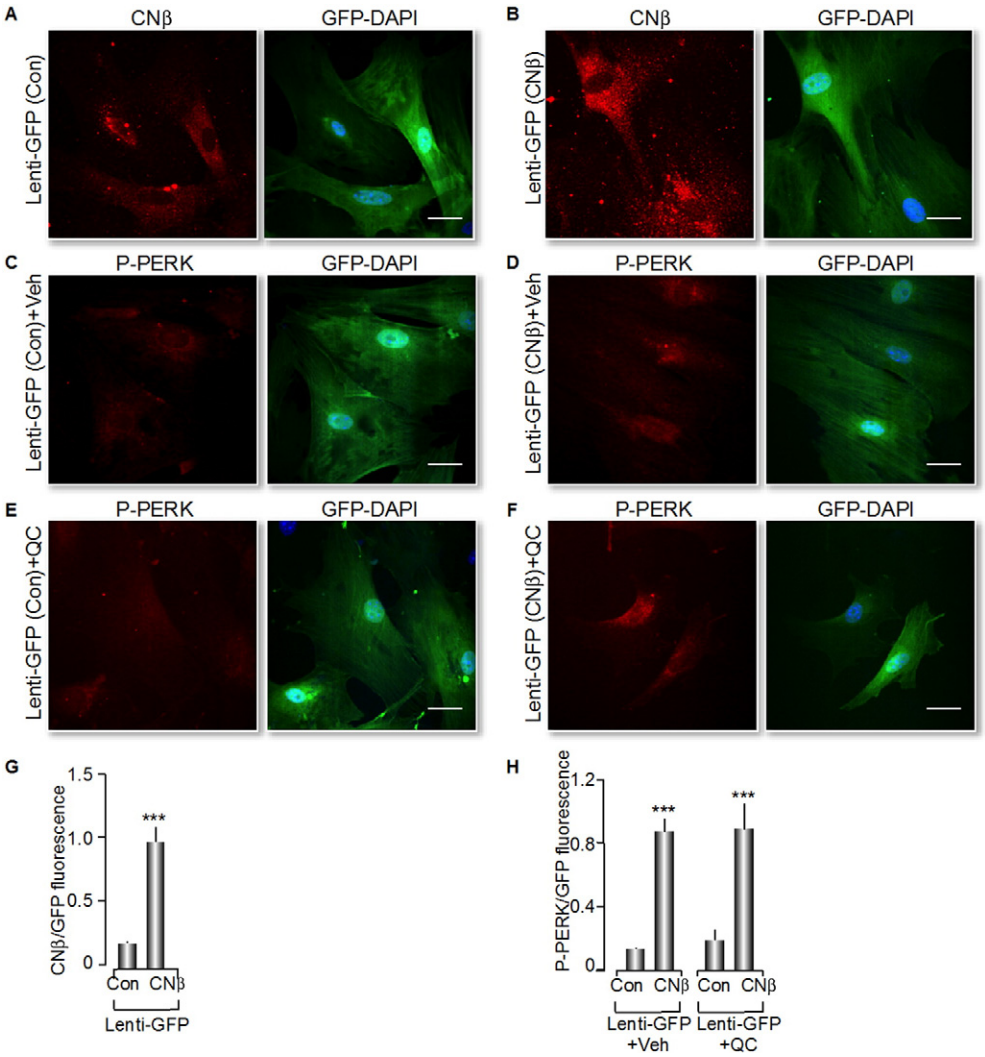

Fig. 5. CNβ induces PERK phosphorylation independent of its phosphatase activity. (A, B) Primary astrocytes cultured from wildtype mice were transduced with pUltra lentivirus containing empty vector (Lenti-GFP Con) or Lenti-GFP (CNβ) and stained for CNβ (red). Nuclei were stained with DAPI (blue). Presence of virus is indicated by GFP (green). (C–F) Infected astrocytes were exposed to DMSO (Veh) or 40 μM of Quercetin (QC) for 20 min. Immuno-cytochemistry was carried out for P-PERK (red) and DAPI (blue). Images were sequentially acquired. Scale bar: 20 μm. (G) Ratio of fluorescence intensity (CNβ/GFP) in (A, B) from three independent experiments in which at least 10 cells were quantified per experiment (mean ± SEM, $^{***}p < 0.001$ by unpaired two-tailed Student's *t*-test). (H) Ratio of fluorescence intensity (P-PERK/GFP) in (C–F) from three independent experiments in which at least 10 cells were quantified per experiment (mean ± SEM, $^{***}p < 0.001$ by one-way ANOVA).

We found that CNβ-PERK interaction occurs within 30 min of ER stress induced by Tg or OGD treatments. We also note that CNβ levels significantly increased in cultured astrocytes under the same conditions. The speed and selectivity of this response, confirmed using chemical-activated dimerization techniques, appears to mimic an acute stress response. These data suggest that CNβ and PERK are only required to be in close proximity to promote PERK autophosphorylation. Since low doses of Tg further increase the efficacy of chemical dimerization, we suggest that Ca^{2+} acts as a PERK cofactor on the cytosolic side of the ER, in agreement with previous findings of our group (Bollo et al., 2010; Paredes et al., 2013).

Moreover, we found that acute brain injury causes more damage in mice when PERK activity is pharmacologically inhibited, which is consistent with published reports showing loss of PERK-enabled neurons more sensitive to stress and decreases viability, probably because the cells are unable to mount an appropriate protective response (Ryu et al., 2002). However, it has also been reported that synaptic failure and neuronal death are associated with persistent global protein synthesis inhibition that is mediated by over-activation of PERK in a prion-diseased mouse model (Moreno et al., 2012; Moreno et al., 2013). It is widely assumed that the duration and/or strength of PERK signaling helps determine cell fate after stress, either leading to cell survival or death (Lin et al., 2009). In response to stress, transient PERK-eIF2α signaling acutely attenuates overall protein synthesis to provide time to resolve and alleviate stress. If unsuccessful, the cell progresses to cell death by inducing the transcription of CHOP that is downstream of PERK-eIF2α pathway (Zinszner et al., 1998; Oyadomari et al., 2002; Pennuto et al., 2008). PERK is well-known to be acutely phosphorylated in neurons within 20 min of ischemia (Kumar et al., 2001). However, our *in vivo* data were obtained 24 h post-stroke and showed that phosphorylation of eIF2α was still significantly increased in reactive astrocytes (Fig. 8). Our data show that eIF2α can remain phosphorylated in astrocytes for prolonged periods without inducing cell death. This holding pattern may represent a different phase or steady-state level of stress mediated by CNβ. It is possible that this long-term, pro-survival stress is specific to CNβ in astrocytes and the isoform-specific interaction of CN/PERK is critical in the outcome of acute brain injury.

As expected, GFAP expression was also significantly increased in WT mice after stroke, but to a much lower extent in $\beta^{-/-}$ mice. GFAP is considered to be a signaling platform that coordinates appropriate

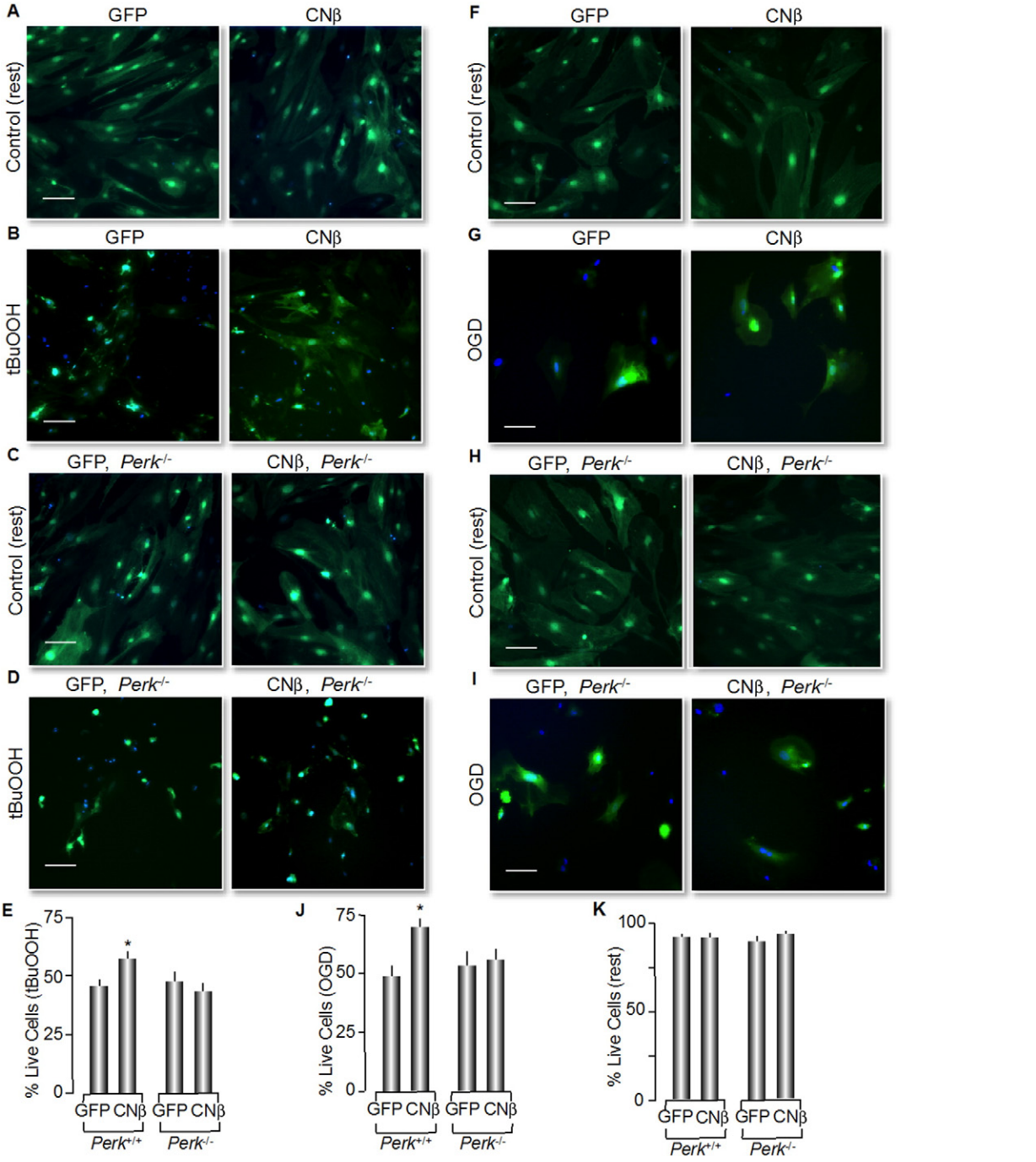

Fig. 6. Lentiviral expression of CNβ increases cell viability of wildtype but not PERK-null astrocytes. (A, C, F, H) Astrocytes cultured from $Perk^{+/+}$ and $Perk^{-/-}$ mice were infected with lentivirus pUltra lenti-GFP or pUltra lenti-GFP (CNβ) (green). Cells in (B, D) were exposed to tBuOOH for 2 h and cells in (G, I) were exposed to OGD for 1 h. Cells in (K) were at rest. Nuclei were stained using Hoechst 33342 (blue). Cells with GFP expression were viable cells. Scale bar: 80 μm. (E, J) Quantification of percent live cells in lentivirus-infected astrocytes in (B, D, G, I) from three independent experiments in which 5 random fields were counted (mean ± SEM, $^{*}p < 0.05$ by one-way ANOVA).

responses in situations related to cellular stress (Kurz et al., 2005). We note that acute brain injury resulted in less reactive gliosis (Tajiri et al., 2004) but larger infarct volumes (Gotoh et al., 2002) in GFAP null mice compared to controls. On the other hand, several reports have also found a link between CN expression levels and reactive gliosis (Norris et al., 2005; Abdul et al., 2009; Lim et al., 2013). Our data further indicate that mice deficient in CNβ exhibit disrupted P-eIF2α, which constitutes the first molecular evidence that the CNβ – PERK pathway could represent an active link between the UPR and reactive gliosis activation. Signaling induces global translation inhibition, but also stimulates the expression of a group of genes *via* the transcription factor, ATF4, when eIF2α is phosphorylated (Lu et al., 2004). Therefore, we speculate that CNβ — PERK — eIF2α pathway positively modulates GFAP expression during astrogliosis induced by acute brain injury.

Overall, our data identify a novel cytoprotective role for the ubiquitous protein, CNβ, which surprisingly appears independent of its phosphatase activity. Our findings also suggest that this signaling pathway may modulate astrogliosis *via* the PERK — eIF2α arm of the integrated stress response/UPR pathway. We anticipate that molecular interventions could be developed that either promote or mimic CNβ binding to PERK, which, in turn, could be used as a potent therapeutic strategy in patients suffering from either trauma or ischemic insults.

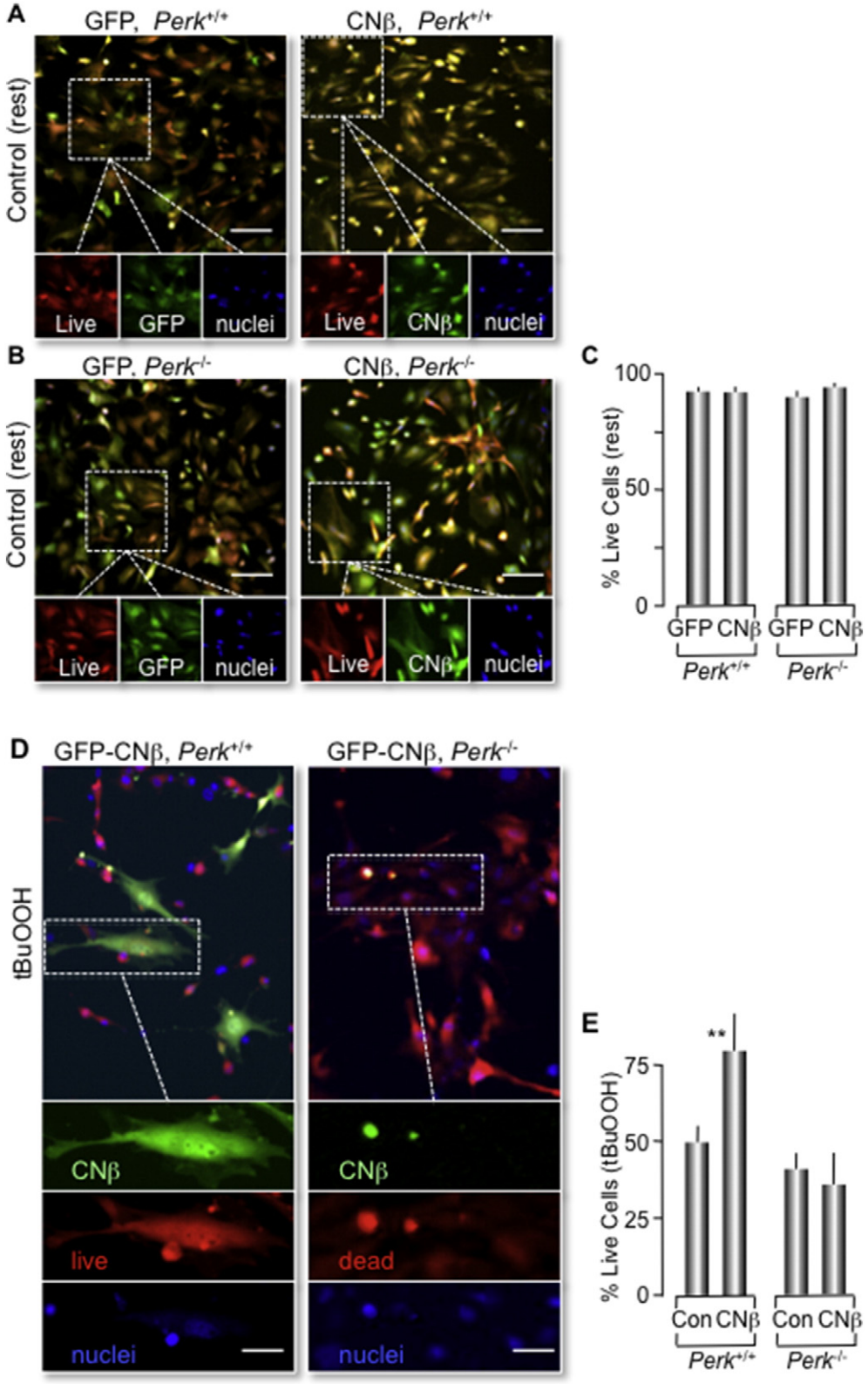

Supplementary Fig. 6. CNβ expression does not cause significant change in cell viability at rest; Transient expression of CNβ increases cell viability of wildtype but not PERK-null astrocytes. (A, B) Images of cultured astrocytes from $Perk^{+/+}$ and $Perk^{-/-}$ mice infected with pUltra lentivirus. Calcein AM (red) stains live cells and Hoescht (blue) stains all nuclei. Cells in green represent successful infection with the lentivirus. Images were acquired on a Nikon inverted TE300 epifluorescence microscope. Scale bar: 200 μm. (C) Quantification of percent live cells in (A, B) from three independent experiments in which 5 random fields were counted (mean ± SEM by one-way ANOVA). (D) Astrocytes cultured from $Perk^{+/+}$ and $Perk^{-/-}$ mice were transiently transfected with GFP-CNβ, treated with of tBuOOH for 2 h, and then stained with calcein AM (red) and Hoechst 33342 (nuclei, blue). Calcein AM-positive cells with good morphology are alive. Scale bar: 20 μm. (E) Quantification of percent live cells in untransfected (Con) and CNβ-transfected astrocytes from four independent experiments in which 5 random fields were counted (mean ± SEM, $^{**}p < 0.01$ by one-way ANOVA).

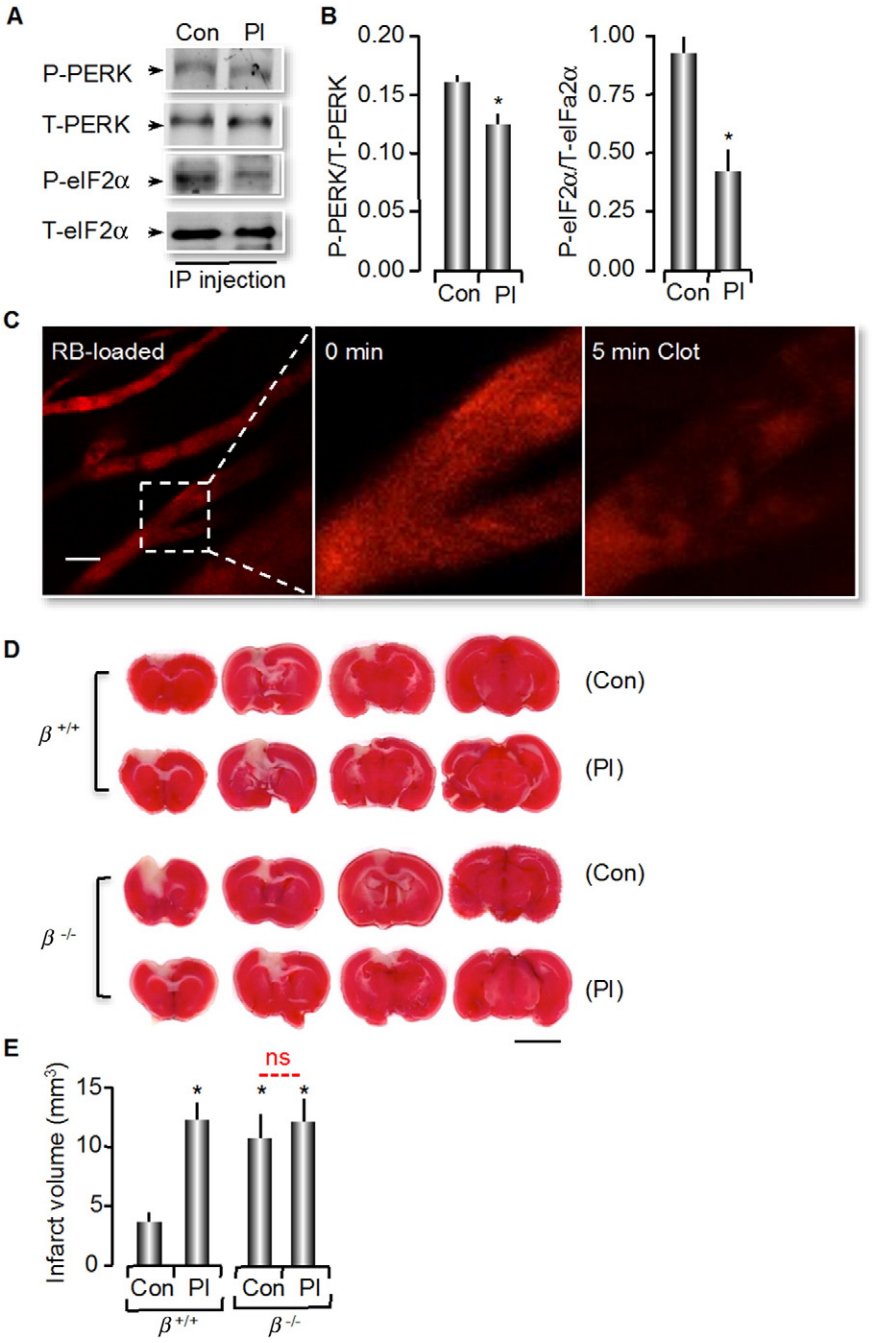

Fig. 7. CNβ null mice exhibit larger infarct size after photothrombotic stroke as compared to CNβ null mice with inhibition of PERK activity. PERK inhibitor (PI) or DMSO (Con) was intraperitoneally injected into CNβ wildtype ($\beta^{+/+}$) and null ($\beta^{-/-}$) mice 12 h before stroke. (A) Homogenized brain lysates of mice at 12 h post-injections were analyzed for *T*-PERK, P-PERK, T-eIF2α and P-eIF2α by immunoblots. (B) Quantification of immunoblots in (A) (n = 3, mean ± SEM, $^*p < 0.05$ by unpaired two-tailed Student's *t*-test). (C) Rose bengal (RB) dye-induced photothrombotic model. Confocal images show that blood vessel lumens were filled with RB dye. Region marked by dashed box was irradiated with 543 nm laser light. After approximately 5 min, a thrombotic clot was formed with the absence of blood flow. Scale bar: 20 μm. (D) Tetrazolium chloride (TTC) staining of serial coronal sections 24 h post-photothrombotic stroke on $\beta^{+/+}$ and $\beta^{-/-}$ mice with DMSO (Con) or PI injection. Scale bar: 5 mm. (E) Quantification of infarct volume 24 h post-stroke in (D) (n = 5, mean ± SEM, $^*p < 0.05$ by one-way ANOVA).

4. Material and methods

4.1. Animals, human tissue, and cell cultures

CNβ heterozygotes on C57BL/6 background were gifts from Dr. Hanna Abboud (University of Texas Health Science Center at San Antonio). Male CNβ knockout mice and wild-type littermates were investigated at 8–10 weeks of age. *Perk* heterozygotes on C57BL/6 background were purchased from the Jackon Laboratory (STOCK *Eif2ak3*^{tm1Dron}/HotaJ) and originally generated by David Ron's laboratory (University of Cambridge) (Harding et al., 2001). Neonates of Perk knockout and wild-type littermates as well as adult male C57BL/6 (4–6 month mice) were used for primary astrocytes culture. All procedures that involved animal subjects were approved by the Institutional Animal Care and Use Committee at the University of Texas Health Science Center at San Antonio.

Human astrocytes were cultured from human brain tissue of a 40 year-old male patient and maintained using the same protocols as

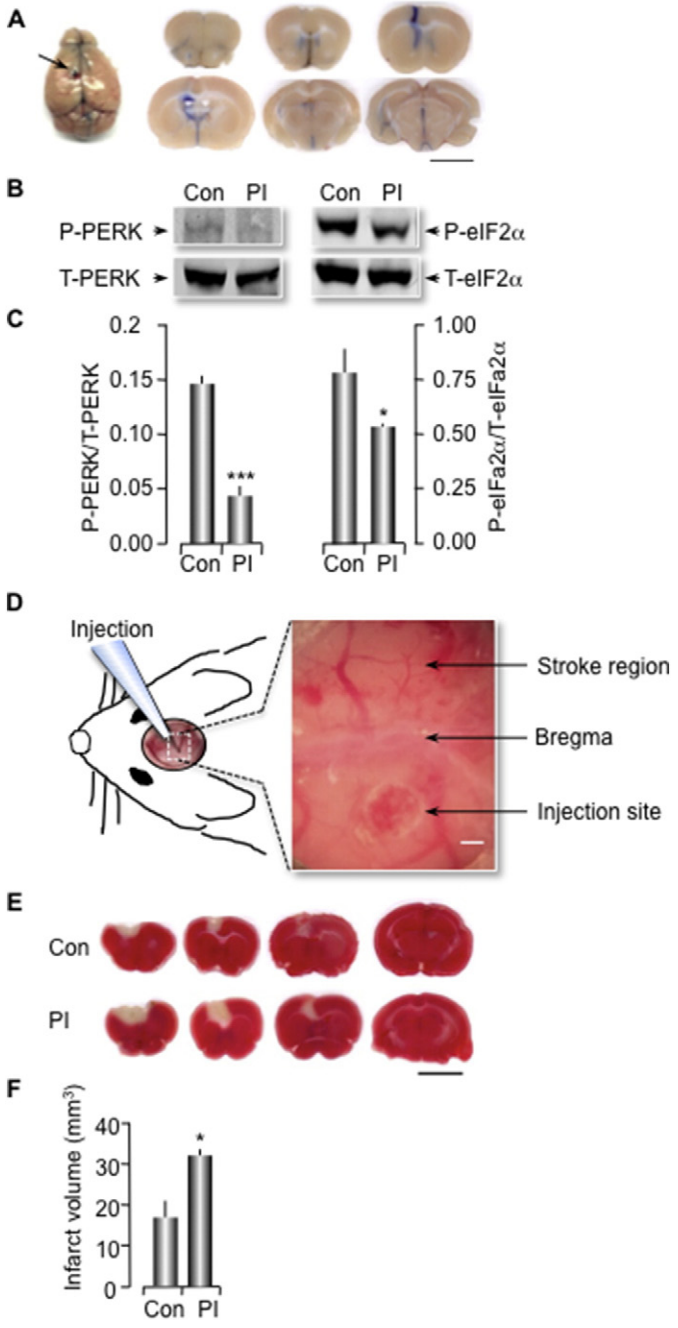

Supplementary Fig. 7. Administration of PERK inhibitor (PI) by lateral ventricle injection decreases PERK activity and results in larger ischemic lesion in mice brain. PERK inhibitor (PI) GSK2656157 or DMSO control (Con) was injected into the lateral ventricle of mice 12 h before stroke. (A) Stereotaxic coordinates were used to target the lateral ventricle. Representative images of the brain after lateral ventricle administration of Evans blue. Black arrow points to the injection site. Coronal sections of the brain show distribution of the blue dye. Scale bar: 5 mm. (B) Homogenized brain lysates of mice after 12 h post administration of PI or Con were analyzed for T-PERK, P-PERK, T-eIF2α and P-eIF2α by immunoblots. (C) Densitometric histograms of (B) (n = 3, mean ± SEM, $^{*}p < 0.05$, $^{***}p < 0.001$ by unpaired two-tailed Student's *t*-test). (D) Schematic diagram of injection through the hole drilled in the exposed cranium (actual image). In the enlarged cranial image on the right, the target region for stroke was exposed by craniotomy on the contralateral side of the PI micro-injection site. Scale bar: 0.5 mm. (E) TTC staining of serial coronal sections 24 h post-stroke in PI or Con groups. Scale bar: 5 mm. (F) Quantification of the infarct volume at 24 h post-stroke in (E) (n = 3 for Con group, n = 4 for PI group, mean ± SEM, $^{*}p < 0.05$, by unpaired two-tailed Student's *t*-test).

mouse astrocyte cultures. The patient who gave his informed consent to the Department of Neurosurgery at the University of Texas Health Science Center San Antonio. The protocols were approved by the local Ethics committee.

Primary astrocyte cultures were prepared as previously described (Lin et al., 2007). The C8D1A astrocyte cell line was purchased (#CRL-2541; ATCC) and maintained in DMEM (#30-2002; ATCC) containing 10% FBS. All cell cultures were incubated at 37 °C in a humid atmosphere containing 5% carbon dioxide (CO_2).

4.2. Immunostaining

We performed immunostaining on cells grown on glass coverslips and fixed with 4% paraformaldehyde or on brain sections (30 μM) as previously described (Holguin et al., 2004). For quercetin (QC, #Q4951; Sigma) treatment, cells were exposed to 40 μM QC or DMSO for 20 min before fixation. Primary antibodies used were rabbit anti-phosphorylated PERK (conjugated to Alexa 647, #bs-3330R-A647; Bioss), rabbit anti-CNα (#13422-1-AP; Proteintech), rabbit anti-CNβ (#07-1439; Millipore), rabbit anti-phosphorylated eIF2α (P-eIF2α, #μA5 — 15133; Thermo scientific) and mouse anti-GFAP (#MAB 360; Millipore). Secondary antibodies (Life Technologies) were added as appropriate. Samples were imaged on an inverted microscope (Nikon TE300, Nikon Instruments Inc.) or a confocal microscope (Olympus FV1000, Olympus; Zeiss LMS 710, Zeiss). The immunofluorescence intensity for each cell was analyzed by NIH Image J software. >10 cells were analyzed in every independent experiment, which was replicated 3 times. For sections, corrected total cell fluorescence intensity was calculated by measuring integrated density minus background reading.

4.3. Immunoprecipitation and co-immunoprecipitation

Cell lysates were incubated with 0.3 mM DSS for 30 min, and microsomal fractions were obtained as described previously (Bollo et al., 2010). Anti-CNβ (5 μg) (#07-068; Millipore, (25) was added. After incubation overnight, the immune complex was washed and the eluted proteins were separated by sodium dodecyl sulfate polyacrylamide gel electrophoresis (SDS-PAGE) and detected by immunoblotting with anti-PERK (PERKUT).

4.4. In vitro kinase activity assay and pull-down assay

In vitro kinase activity assay and pull-down assay were performed as described previously (Bollo et al., 2010).

4.5. Western blot

Western blot analysis was performed using 30 μg of total protein in cell lysates. The following antibodies were used in this study: anti-CNα (#07-067; Millipore), anti-CNβ (#07-068;Millipore), anti-actin (#MAB1501; Millipore), anti-CN-B (#07-069; Millipore), and anti-GFP (#111258; Abcam), anti-P-PERK (#3179; Cell signaling Technology), anti-T-PERK (#3192; Cell signaling Technology), anti-P-eIF2α (#3597; Cell signaling Technology), and anti-T-eIF2α (#9722; Cell signaling Technology).

4.6. ER tracker imaging

Cultured human astrocytes expressing CFP-FRB-cb5 were washed with HBSS and then loaded with 1uM of ER-tracker™ blue-white DPX (#E-12353; Life technologies) for 30 min at 37 °C. After incubation, cells were washed with HBSS and then observed using a Nikon 60× oil immersion objective (NA 1.2) on Olympus FV-1000 confocal microscope.

4.7. Measurement of Ca^{2+} signal

Human astrocytes were incubated with the mixture of Fluo-4 AM (#F14217; Life technologies) and pluronic acid F-127 (#P3000MP; Life technologies) for 30 min at the room temperature. Cells were washed

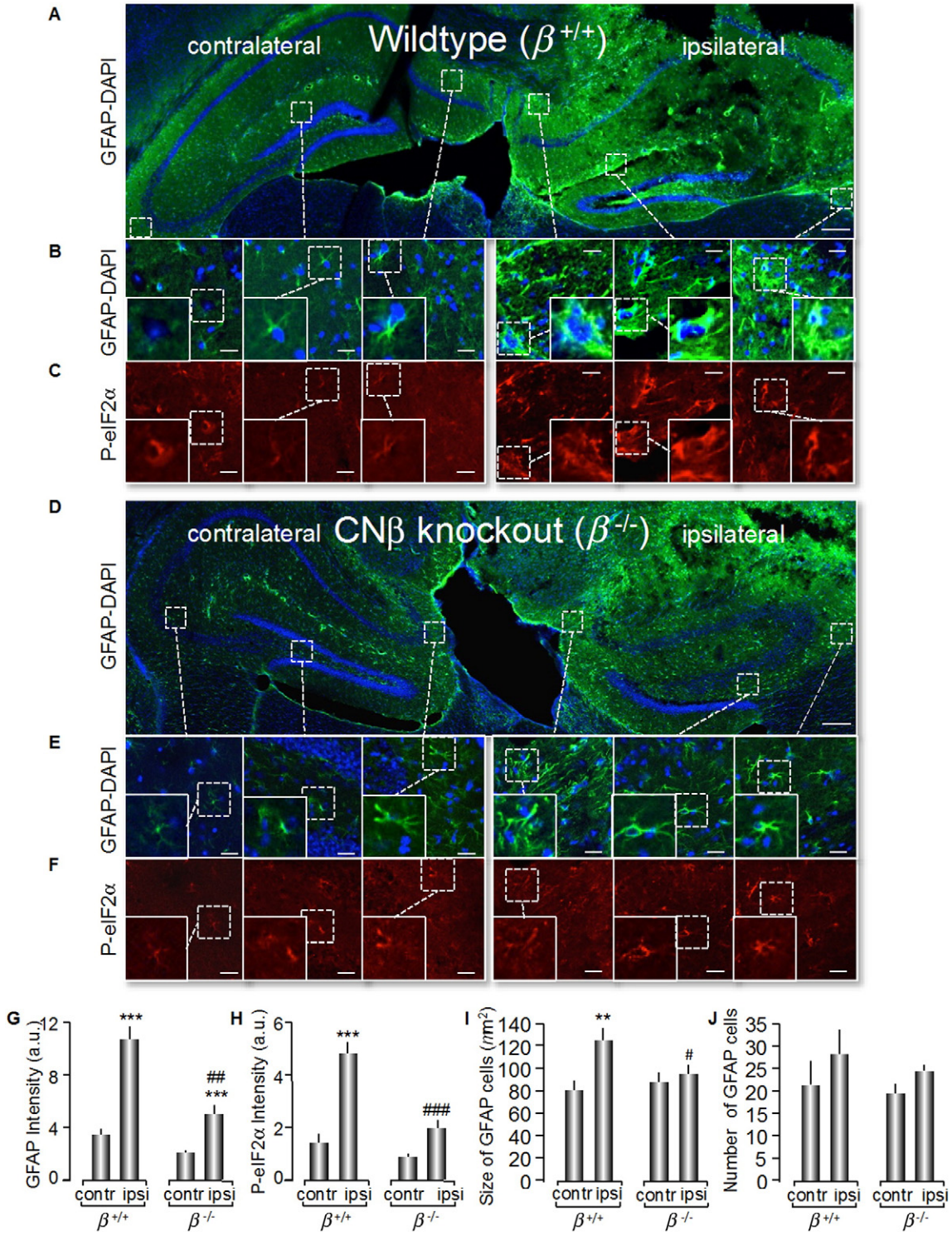

Fig. 8. $\beta^{+/+}$, not $\beta^{-/-}$ mice, exhibit enlarged astrocytes as well as up-regulated P-eIF2α in reactive astrocytes after stroke. Mouse brains harvested at post 24 h of stroke were sectioned and stained with antibodies against P-eIF2α (red), GFAP (green) and DAPI (nuclei, blue). Montage images were acquired on a Zeiss LMS 710 confocal microscopy with a Nikon 20× objective. (A, D) The $\beta^{+/+}$ and $\beta^{-/-}$ brain sections with GFAP and DAPI staining. (B, E) The high magnification of images from the dashed boxes in A and D, respectively. (C, F) The brain sections from B and E in P-eIF2α staining, respectively. (G-J) Quantification of fluorescence intensities of GFAP and P-eIF2α in astrocytes, the size and the number of GFAP positive astrocytes (n = 3, four random regions analyzed from each side, mean ± SEM). $^{**}p < 0.01$ and $^{***}p < 0.001$, compared with the contralateral (contr) side; $^{\#}p < 0.05$, $^{\#\#}p < 0.01$ and $^{\#\#\#}p < 0.001$, compared with the ipsilateral (ipsi) side of $\beta^{+/+}$ respectively, by 1-way ANOVA. Scale bar: 250 μm (A, D); 20 μm (B, C, E, F).

out with PBS and then incubated for additional 30 min to allow complete de-esterification of intracellular AM esters. After incubation, cells were treated with 25 nM of Tg. Confocal microscopy images were acquired every 5 min for 30 min using Nikon 60× oil immersion objective (NA 1.24) under the Nikon swept field confocal microscope (Nikon instruments Inc., Melville). F is the mean fluorescence intensity of Fluo-4 measured throughout the regions of interest (ROIs). F0 represents the intensity at the time 0 and ΔF represents a change in intensity at

different time points compared to the time 0. At least 3 cells were analyzed in each independent experiment, which was replicated for three times.

4.8. Stereotaxic injection into the mouse lateral ventricle

Male B6 Albino mice (8 weeks, Charles River laboratories) were anesthetized with isoflurane (3% induction and 1% maintenance; #NDC 13985-030-60, Vetone,) in 100% oxygen and placed into a stereotaxic frame. The skull was exposed, a hole was drilled, and 1 μl of Evans (#E2129; Sigma) was injected into the left lateral ventricle, using a 10 μl Hamilton syringe to establish our initial coordinates. The following stereotactic coordinates were used: −1.0 mm anterior-posterior (AP), −1.0 mm medial-lateral (ML) and −2.0 mm dorsalventral (DV) to the bregma (Stanley et al., 2004). Using the same coordinates, a total volume of 1 μl of GSK2656157 (2 mM in DMSO, #406230; MedKoo Bioscience) or DMSO (Con) was injected into the lateral ventricle.

4.9. Traumatic brain injury (TBI) and Nissl staining

A controlled closed cortical impact (CCCI) model was used to generate a moderate TBI as previously described (Talley Watts et al., 2013). In brief, mice were anesthetized, the skull exposed and a pneumatic impact device was used to produce a moderate TBI over the somatosensory cortex (Talley Watts et al., 2013). The calibrated impact was 4.5 m/s and a depth of 2 mm. Scalp incisions were closed and mice were monitored until fully awake. Twenty-four hours after the initial trauma, mice were perfused with 4% paraformaldehyde (#RT157-4; Electron Microscopy Sciences) before brains were harvested and sectioned. Nissl staining was used to reveal histology of the cortical lesion area as described previously (Talley Watts et al., 2013). Lesion volume was calculated as the sum of lesion areas in consecutive sections over the rostro-caudal extension of the brain. Image J was used to determine the area of each soma.

4.10. Cortical photothrombosis and Triphenyl-tetrazolium chloride (TTC) staining

Photothrombotic stroke was induced by focusing light on the cortex of Rose Bengal (RB; #330000; Sigma) tail-vein injected mice (Zheng et al., 2010). TTC (#17779 FLUKA; Sigma) staining was used to evaluate the infarct size at 24 hour post-RB-induced-photothrombosis (Zheng et al., 2010). Infarct volume was calculated by multiplying the sum of the infarcted areas (mm^2) of various sequential coronal sections by slice thickness (1 mm).

4.11. ER stress induction

Thapsigargin (1 μM) (Tg, #T9033; Sigma), *tert*-butyl hydrogen peroxide (100 μM) (tBuOOH; #B-2633; Sigma), and oxygen glucose deprivation (OGD) were used as stressors in this study. OGD was performed as previously described (Badiola et al., 2011). Briefly, cultured primary astrocytes were washed twice, incubated in glucose-free DMEM, (#11966025; Life Technologies) and transferred to an anaerobic chamber filled with a gas mixture of 95% nitrogen and 5% CO_2 at 37 °C.

4.12. Recombinant protein cross-linking assay

GST-cPERK, MBP-cPERK, 6His-CNβ, 6His-CNα and 6His-CN-B protein purifications were performed as previously described (Bollo et al., 2010; Li & Sousa, 2012). All recombinant proteins, even at concentrations of 1.0 to 1.2 mg/ml, showed no absorbance from 310 to 340 nm in absorption spectra (220 to 350 nm), supporting the absence of aggregates in the solution. Recombinant proteins His-CNβ and GST-cPERK (or MBP-cPERK) were incubated in the presence of 0.3 mM DSS cross-linker (#21658; Thermo Scientific,) for 30 min at room temperature. Reactions were quenched in 1 M tris (hydroxymethyl) aminomethane hydrochloride (Tris HCl; pH, 7.5) for 15 min at room temperature. The protein complexes were analyzed by SDS-PAGE (4% to 12%) and detected by immunoblotting either with anti-PERK antibody (PERKUT) or with anti-CNβ (#07-068; Millipore).

4.13. Rapamycin-inducible dimerization assay

This assay was performed as previously described (Komatsu et al., 2010). Briefly, FKBP was fused with YFP-CNβ (effector unit) and FRB was fused with CFP-cytochrome *b*5 (Cb5) (anchor unit). Transfected human astrocytes were treated with 100 nM rapamycin (#9904; Cell Signaling) to induce dimerization events for 30 min. A second treatment paradigm was rapamycin (10 min) followed by Tg (25 nM; 20 min). DMSO with or without Tg was used as a control reagent. Cells were immediately fixed after 30 min of treatment and immunostained with anti-P-PERK antibody conjugated to Alexa 647 (#bs-3330R-A647; Bioss). >20 transfected cells were analyzed in each group.

4.14. Lentiviral vector production and transduction

A third generation, multicistronic lentiviral vector was purchased (pUltra plasmid 24129; Addgene). The cDNA encoding CNβ was subcloned into the *Xba*I/*Bam*HI site and the cDNA encoding CN-B was subcloned into the *Nhe*I site in the vector (pUltra). The constructed GFP-P2A-CNβ-T2 A-CN-B can be used to express GFP, CNβ, and CN-B proteins from a single open reading frame by efficient cleavage within the 2A peptide sequence.

Lentiviral vectors were produced as described previously (Zufferey et al., 1997). Briefly, pUltra-CNβ-CN-B (lenti-GFP (CNβ)) or pUltra control (lenti-GFP) were cotransfected with the second generation packaging plasmid, psPAX2, and the envelope plasmid, pMD2.G using Lipofectamine LTX into HEK293FT cells. The supernatant medium was collected 4 days after transfection and concentrated (Lenti-X concentrator, #631231;Clontech) using the manufacturer's protocol. The viral particle titer was determined by transduction of HEK293 cells followed by fluorescence activated cell sorting (FACS) analysis.

Primary isolated astrocytes from $Perk^{-/-}$ and $Perk^{+/+}$ siblings were plated at 5000 cells per well in a 24-well plate and infected with the viral particles (multiplicity of infection, 200) in the presence of a transduction reagent (Transdux, #LV850A-1; System Biosciences) by centrifugation at 800 ×*g* for 1.5 h. Cells were placed in an incubator (5% carbon dioxide; 37 °C) overnight and observed every 24 h. The highest expression level of GFP was usually visualized 5 to 7 days after infection.

4.15. Cell viability assay

Sensitivity of astrocytes to oxidative stress was assessed by exposing cultures to tBuOOH for 2 h or OGD for 1 h. Cells were stained with Hoechst 33342 (10 μg/ml, #H-3570; Life Technologies) to label all cell nuclei and/or calcein red-orange (CellTrace AM, 2 μM, #C34851; Life Technologies) to identify live cells that maintained their plasma membrane integrity. Cells with good morphology were counted as live and cells with beading were counted as dead cells. For pUltra virus-infected cells, cells with GFP expression represented viable cells. Images were acquired on an inverted microscope (TE300; Nikon). We calculated percent live cells as the number of viable cells divided by the total number of cells labeled with Hoechst 33342 (#H3570; Life technologies). We counted 5 random fields in every independent experiment, which was replicated a minimum of three times.

4.16. Statistical analysis

Results are presented as means of independent replicates of experiments ± SEM. Comparisons were made with two-tailed Student's *t*-test, one-way analysis of variance (ANOVA), and Newman-Keuls test.

Differences were considered as significant at $p < 0.05$, moderately significant at $p < 0.01$, or highly significant at $p < 0.001$.

The following are the supplementary data related to this article.

Funding

This work was supported by the National Institutes of Health (NS085732, 2013 Subaward Agreement 155726/155448; UTHASCA/Institute Ferreyra), Ministerio de Ciencia y Tecnologia de Cordoba, Argentina (PID-2010) and Fulbright/CONICET (Argentina) Fellowship.

Conflict of interest

The authors declare that they have no conflict of interest.

Acknowledgments

We thank Dr. Naomi Sayre and Shane M Sprague for their help with the traumatic brain injury model, Dr. Rui Sousa and Dr. Yifeng Liu for MBP-cPERK and CN purification, Dr. Ramaswamy Sharma for his critical reading and thoughtful editing and Brian Stovenken for his comments on the manuscript. We are especially grateful to Dr. Takanari Inoue from Johns Hopkins University for providing CFP-FRB-cb5 and YFP-FKBP constructs.

References

Abdul, H.M., Sama, M.A., Furman, J.L., Mathis, D.M., Beckett, T.L., Weidner, A.M., et al., 2009 Oct 14. Cognitive decline in Alzheimer's disease is associated with selective changes in calcineurin/NFAT signaling. J. Neurosci. 29 (41), 12957–12969 (PubMed PMID: 19828810. Pubmed Central PMCID: 2782445).

Agostinho, P., Lopes, J.P., Velez, Z., Oliveira, C.R., 2008 Mayy. Overactivation of calcineurin induced by amyloid-beta and prion proteins. Neurochem. Int. 52 (6), 1226–1233 (PubMed PMID: 18295934).

Axten, J.M., Medina, J.R., Feng, Y., Shu, A., Romeril, S.P., Grant, S.W., et al., 2012 Aug 23. Discovery of 7-methyl-5-(1-{[3-(trifluoromethyl)phenyl]acetyl}-2,3-dihydro-1H-indol-5-yl)-7H-p yrrolo[2,3-d]pyrimidin-4-amine (GSK2606414), a potent and selective first-in-class inhibitor of protein kinase R (PKR)-like endoplasmic reticulum kinase (PERK). J. Med. Chem. 55 (16), 7193–7207 (PubMed PMID: 22827572).

Badiola, N., Penas, C., Minano-Molina, A., Barneda-Zahonero, B., Fado, R., Sanchez-Opazo, G., et al., 2011. Induction of ER stress in response to oxygen-glucose deprivation of cortical cultures involves the activation of the PERK and IRE-1 pathways and of caspase-12. Cell Death Dis. 2, e149 (PubMed PMID: 21525936. Pubmed Central PMCID: 3122062. Epub 2011/04/29).

Bertolotti, A., Zhang, Y., Hendershot, L.M., Harding, H.P., Ron, D., 2000 Junn. Dynamic interaction of BiP and ER stress transducers in the unfolded-protein response. Nat. Cell Biol. 2 (6), 326–332 (PubMed PMID: 10854322. Epub 2000/06/15. eng).

Bollo, M., Paredes, R.M., Holstein, D., Zheleznova, N., Camacho, P., Lechleiter, J.D., 2010. Calcineurin interacts with PERK and dephosphorylates calnexin to relieve ER stress in mammals and frogs. PLoS One 5 (8), e11925 (PubMed PMID: 20700529. Pubmed Central PMCID: 2916823. Epub 2010/08/12).

Brostrom, M.A., Brostrom, C.O., 2003 Oct-Novv. Calcium dynamics and endoplasmic reticular function in the regulation of protein synthesis: implications for cell growth and adaptability. Cell Calcium 34 (4–5), 345–363 (PubMed PMID: 12909081. Epub 2003/08/12. eng).

Ellgaard, L., Helenius, A., 2003 Marr. Quality control in the endoplasmic reticulum. Nat. Rev. Mol. Cell Biol. 4 (3), 181–191 (PubMed PMID: 12612637. Epub 2003/03/04).

Farook, J.M., Shields, J., Tawfik, A., Markand, S., Sen, T., Smith, S.B., et al., 2013. GADD34 induces cell death through inactivation of Akt following traumatic brain injury. Cell Death Dis. 4, e754 (PubMed PMID: 23907468. Pubmed Central PMCID: 3763442. Epub 2013/08/03).

Fernandez, A.M., Fernandez, S., Carrero, P., Garcia-Garcia, M., Torres-Aleman, I., 2007 Aug 15. Calcineurin in reactive astrocytes plays a key role in the interplay between proinflammatory and anti-inflammatory signals. J. Neurosci. 27 (33), 8745–8756 (PubMed PMID: 17699657. Epub 2007/08/19).

Gotoh, T., Oyadomari, S., Mori, K., Mori, M., 2002 Apr 5. Nitric oxide-induced apoptosis in RAW 264.7 macrophages is mediated by endoplasmic reticulum stress pathway involving ATF6 and CHOP. J. Biol. Chem. 277 (14), 12343–12350 (PubMed PMID: 11805088).

Han, D., Lerner, A.G., Vande Walle, L., Upton, J.P., Xu, W., Hagen, A., et al., 2009 Aug 7. IRE1alpha kinase activation modes control alternate endoribonuclease outputs to determine divergent cell fates. Cell 138 (3), 562–575 (PubMed PMID: 19665977. Pubmed Central PMCID: 2762408. Epub 2009/08/12).

Harding, H.P., Zeng, H., Zhang, Y., Jungries, R., Chung, P., Plesken, H., et al., 2001 Junn. Diabetes mellitus and exocrine pancreatic dysfunction in perk−/− mice reveals a role for translational control in secretory cell survival. Mol. Cell 7 (6), 1153–1163 (PubMed PMID: 11430819).

Hashimoto, T., Kawamata, T., Saito, N., Sasaki, M., Nakai, M., Niu, S., et al., 1998 Marr. Isoform-specific redistribution of calcineurin A alpha and A beta in the hippocampal CA1 region of gerbils after transient ischemia. J. Neurochem. 70 (3), 1289–1298 (PubMed PMID: 9489752).

He, S., Yaung, J., Kim, Y.H., Barron, E., Ryan, S.J., Hinton, D.R., 2008 Mayy. Endoplasmic reticulum stress induced by oxidative stress in retinal pigment epithelial cells. Graefes Arch. Clin. Exp. Ophthalmol. 246 (5), 677–683 (PubMed PMID: 18278507. Epub 2008/02/19).

Holguin, A., Paxinos, E., Hertogs, K., Womac, C., Soriano, V., 2004 Novv. Impact of frequent natural polymorphisms at the protease gene on the in vitro susceptibility to protease inhibitors in HIV-1 non-B subtypes. J. Clin. Virol. 31 (3), 215–220 (PubMed PMID: 15465415).

Honsho, M., Mitoma, J.Y., Ito, A., 1998 Aug 14. Retention of cytochrome b5 in the endoplasmic reticulum is transmembrane and luminal domain-dependent. J. Biol. Chem. 273 (33), 20860–20866 (PubMed PMID: 9694832. Epub 1998/08/08).

Ji, X., Zhang, P., Armstrong, R.N., Gilliland, G.L., 1992 Oct 27. The three-dimensional structure of a glutathione S-transferase from the mu gene class. Structural analysis of the binary complex of isoenzyme 3-3 and glutathione at 2.2-A resolution. Biochemistry 31 (42), 10169–10184 (PubMed PMID: 1420139. Epub 1992/10/27).

Kaufman, R.J., 2004 Marr. Regulation of mRNA translation by protein folding in the endoplasmic reticulum. Trends Biochem. Sci. 29 (3), 152–158 (PubMed PMID: 15003273. Epub 2004/03/09. eng).

Klee, C.B., Krinks, M.H., 1978 Jan 10. Purification of cyclic 3′,5′-nucleotide phosphodiesterase inhibitory protein by affinity chromatography on activator protein coupled to sepharose. Biochemistry 17 (1), 120–126 (PubMed PMID: 201280).

Klee, C.B., Ren, H., Wang, X., 1998 May 29. Regulation of the calmodulin-stimulated protein phosphatase, calcineurin. J. Biol. Chem. 273 (22), 13367–13370 (PubMed PMID: 9593662).

Komatsu, T., Kukelyansky, I., McCaffery, J.M., Ueno, T., Varela, L.C., Inoue, T., 2010 Marr. Organelle-specific, rapid induction of molecular activities and membrane tethering. Nat. Methods 7 (3), 206–208 (PubMed PMID: 20154678. Pubmed Central PMCID: 2860863. Epub 2010/02/16).

Kovacs, G.G., Zsembery, A., Anderson, S.J., Komlosi, P., Gillespie, G.Y., Bell, P.D., et al., 2005 Augg. Changes in intracellular Ca^{2+} and pH in response to thapsigargin in human glioblastoma cells and normal astrocytes. Am. J. Physiol. Cell Physiol. 289 (2), C361–C371 (PubMed PMID: 15800052. Epub 2005/04/01).

Krajewska, M., Xu, L., Xu, W., Krajewski, S., Kress, C.L., Cui, J., et al., 2011 Jan 25. Endoplasmic reticulum protein BI-1 modulates unfolded protein response signaling and protects against stroke and traumatic brain injury. Brain Res. 1370, 227–237 (PubMed PMID: 21075086. Pubmed Central PMCID: 3019258. Epub 2010/11/16).

Kumar, R., Azam, S., Sullivan, J.M., Owen, C., Cavener, D.R., Zhang, P., et al., 2001 Junn. Brain ischemia and reperfusion activates the eukaryotic initiation factor 2alpha kinase, PERK. J. Neurochem. 77 (5), 1418–1421 (PubMed PMID: 11389192).

Kumar, R., Krause, G.S., Yoshida, H., Mori, K., DeGracia, D.J., 2003 Aprr. Dysfunction of the unfolded protein response during global brain ischemia and reperfusion. J. Cereb. Blood Flow Metab. 23 (4), 462–471 (PubMed PMID: 12679723. Epub 2003/04/08).

Kuno, T., Mukai, H., Ito, A., Chang, C.D., Kishima, K., Saito, N., et al., 1992 Mayy. Distinct cellular expression of calcineurin A alpha and A beta in rat brain. J. Neurochem. 58 (5), 1643–1651 (PubMed PMID: 1313851).

Kurz, J.E., Parsons, J.T., Rana, A., Gibson, C.J., Hamm, R.J., Churn, S.B., 2005 Aprr. A significant increase in both basal and maximal calcineurin activity following fluid percussion injury in the rat. J. Neurotrauma 22 (4), 476–490 (PubMed PMID: 15853464. Epub 2005/04/28)..

Lei, H., Luo, J., Tong, L., Peng, L.Q., Qi, Y., Jia, Z.G., et al., 2011 Aug 1. Quercetin binds to calcineurin at a similar region to cyclosporin A and tacrolimus. Food Chem. 127 (3), 1169–1174 (PubMed PMID: 25214110).

Li, Y., Sousa, R., 2012 Marr. Expression and purification of *E. coli* BirA biotin ligase for in vitro biotinylation. Protein Expr. Purif. 82 (1), 162–167 (PubMed PMID: 22227598. Pubmed Central PMCID: 3288220. Epub 2012/01/10).

Lim, D., Iyer, A., Ronco, V., Grolla, A.A., Canonico, P.L., Aronica, E., et al., 2013 Jull. Amyloid beta deregulates astroglial mGluR5-mediated calcium signaling via calcineurin and Nf-kB. Glia 61 (7), 1134–1145 (PubMed PMID: 23616440).

Lin, D.T., Wu, J., Holstein, D., Upadhyay, G., Rourk, W., Muller, E., et al., 2007 Jann. Ca^{2+} signaling, mitochondria and sensitivity to oxidative stress in aging astrocytes. Neurobiol. Aging 28 (1), 99–111 (PubMed PMID: 16359757. Epub 2005/12/20).

Lin, J.H., Li, H., Zhang, Y., Ron, D., Walter, P., 2009. Divergent effects of PERK and IRE1 signaling on cell viability. PLoS One 4 (1), e4170 (PubMed PMID: 19137072. Pubmed Central PMCID: 2614882. Epub 2009/01/13).

Lu, P.D., Harding, H.P., Ron, D., 2004 Oct 11. Translation reinitiation at alternative open reading frames regulates gene expression in an integrated stress response. J. Cell Biol. 167 (1), 27–33 (PubMed PMID: 15479734. Pubmed Central PMCID: 2172506).

Ma, K., Vattem, K.M., Wek, R.C., 2002 May 24. Dimerization and release of molecular chaperone inhibition facilitate activation of eukaryotic initiation factor-2 kinase in response to endoplasmic reticulum stress. J. Biol. Chem. 277 (21), 18728–18735 (PubMed PMID: 11907036. Epub 2002/03/22. eng).

Moreno, J.A., Radford, H., Peretti, D., Steinert, J.R., Verity, N., Martin, M.G., et al., 2012 May 24. Sustained translational repression by eIF2alpha-P mediates prion neurodegeneration. Nature 485 (7399), 507–511 (PubMed PMID: 22622579. Pubmed Central PMCID: 3378208. Epub 2012/05/25).

Moreno JA, Halliday M, Molloy C, Radford H, Verity N, Axten JM, et al. Oral treatment targeting the unfolded protein response prevents neurodegeneration and clinical disease in prion-infected mice. Sci. Transl. Med. 2013 Oct 9; 5(206):206ra138. (PubMed PMID: 24107777. Epub 2013/10/11).

Mounir Z, Krishnamoorthy JL, Wang S, Papadopoulou B, Campbell S, Muller WJ, et al. Akt determines cell fate through inhibition of the PERK-eIF2alpha phosphorylation pathway. Sci. Signal. 2011 Sep 27;4(192):ra62. (PubMed PMID: 21954288. Pubmed Central PMCID: 3752779).

Nakka, V.P., Prakash-Babu, P., Vemuganti, R., 2014 Decc. Crosstalk between endoplasmic reticulum stress, oxidative stress, and autophagy: potential therapeutic targets for acute CNS injuries. Mol. Neurobiol. 9 (PubMed PMID: 25482050).

Nedergaard, M., 1994 Mar 25. Direct signaling from astrocytes to neurons in cultures of mammalian brain cells. Science 263 (5154), 1768–1771 (PubMed PMID: 8134839).

Norris, C.M., Kadish, I., Blalock, E.M., Chen, K.C., Thibault, V., Porter, N.M., et al., 2005 May 4. Calcineurin triggers reactive/inflammatory processes in astrocytes and is upregulated in aging and Alzheimer's models. J. Neurosci. 25 (18), 4649–4658 (PubMed PMID: 15872113. Pubmed Central PMCID: 1201418. Epub 2005/05/06).

Owen, C.R., Kumar, R., Zhang, P., McGrath, B.C., Cavener, D.R., Krause, G.S., 2005 Sepp. PERK is responsible for the increased phosphorylation of eIF2alpha and the severe inhibition of protein synthesis after transient global brain ischemia. J. Neurochem. 94 (5), 1235–1242 (PubMed PMID: 16000157. Epub 2005/07/08. eng).

Oyadomari, S., Koizumi, A., Takeda, K., Gotoh, T., Akira, S., Araki, E., et al., 2002 Febb. Targeted disruption of the Chop gene delays endoplasmic reticulum stress-mediated diabetes. J. Clin. Invest. 109 (4), 525–532 (PubMed PMID: 11854325. Pubmed Central PMCID: 150879. Epub 2002/02/21).

Paredes, R.M., Bollo, M., Holstein, D., Lechleiter, J.D., 2013 Aprr. Luminal Ca^{2+} depletion during the unfolded protein response in Xenopus oocytes: cause and consequence. Cell Calcium 53 (4), 286–296 (PubMed PMID: 23415071. Pubmed Central PMCID: 3594557. Epub 2013/02/19).

Parker, M.W., Lo Bello, M., Federici, G., 1990 May 20. Crystallization of glutathione S-transferase from human placenta. J. Mol. Biol. 213 (2), 221–222 (PubMed PMID: 2342105. (Epub 1990/05/20).

Paschen, W., 2004 Aprr. Endoplasmic reticulum dysfunction in brain pathology: critical role of protein synthesis. Curr. Neurovasc. Res. 1 (2), 173–181 (PubMed PMID: 16185192).

Pennuto, M., Tinelli, E., Malaguti, M., Del Carro, U., D'Antonio, M., Ron, D., et al., 2008 Feb 7. Ablation of the UPR-mediator CHOP restores motor function and reduces demyelination in Charcot-Marie-Tooth 1B mice. Neuron 57 (3), 393–405 (PubMed PMID: 18255032. Pubmed Central PMCID: 2267889. Epub 2008/02/08).

Polley, S., Huang, D.B., Hauenstein, A.V., Fusco, A.J., Zhong, X., Vu, D., et al., 2013. A structural basis for IkappaB kinase 2 activation via oligomerization-dependent trans autophosphorylation. PLoS Biol. 11 (6), e1001581 (PubMed PMID: 23776406. Pubmed Central PMCID: 3678999. Epub 2013/06/19).

Polli, J.W., Billingsley, M.L., Kincaid, R.L., 1991 Nov 19. Expression of the calmodulin-dependent protein phosphatase, calcineurin, in rat brain: developmental patterns and the role of nigrostriatal innervation. Brain Res. Dev. Brain Res. 63 (1–2), 105–119 (PubMed PMID: 1665105. Epub 1991/11/19. eng).

Pyrzynska, B., Lis, A., Mosieniak, G., Kaminska, B., 2001 Aprr. Cyclosporin A-sensitive signaling pathway involving calcineurin regulates survival of reactive astrocytes. Neurochem. Int. 38 (5), 409–415 (PubMed PMID: 11222921. Epub 2001/02/27).

Reese, L.C., Zhang, W., Dineley, K.T., Kayed, R., Taglialatela, G., 2008 Decc. Selective induction of calcineurin activity and signaling by oligomeric amyloid beta. Aging Cell 7 (6), 824–835 (PubMed PMID: 18782350. Pubmed Central PMCID: 2954114).

Richarme, G., 1982 Mar 30. Associative properties of the *Escherichia coli* galactose binding protein and maltose binding protein. Biochem. Biophys. Res. Commun. 105 (2), 476–481 (PubMed PMID: 7046749. Epub 1982/03/30).

Ron, D., Walter, P., 2007 Jull. Signal integration in the endoplasmic reticulum unfolded protein response. Nat. Rev. Mol. Cell Biol. 8 (7), 519–529 (PubMed PMID: 17565364).

Ryu, E.J., Harding, H.P., Angelastro, J.M., Vitolo, O.V., Ron, D., Greene, L.A., 2002 Dec 15. Endoplasmic reticulum stress and the unfolded protein response in cellular models of Parkinson's disease. J. Neurosci. 22 (24), 10690–10698 (PubMed PMID: 12486162).

Shioda, N., Fukunaga, K., 2011 Jann. Functional roles of constitutively active calcineurin in delayed neuronal death after brain ischemia. Yakugaku Zasshi 131 (1), 13–20 (PubMed PMID: 21212608).

Stanley, S.K., Ghanayem, A.J., Voronov, L.I., Havey, R.M., Paxinos, O., Carandang, G., et al., 2004 Nov 15. Flexion-extension response of the thoracolumbar spine under compressive follower preload. Spine 29 (22), E510–E514 (PubMed PMID: 15543052).

Stichel, C.C., Muller, H.W., 1998 Octt. The CNS lesion scar: new vistas on an old regeneration barrier. Cell Tissue Res. 294 (1), 1–9 (PubMed PMID: 9724451).

Tajiri, S., Oyadomari, S., Yano, S., Morioka, M., Gotoh, T., Hamada, J.I., et al., 2004 Aprr. Ischemia-induced neuronal cell death is mediated by the endoplasmic reticulum stress pathway involving CHOP. Cell Death Differ. 11 (4), 403–415 (PubMed PMID: 14752508).

Talley Watts, L., Sprague, S., Zheng, W., Garling, R.J., Jimenez, D., Digicaylioglu, M., et al., 2013 Jan 1. Purinergic 2Y1 receptor stimulation decreases cerebral edema and reactive gliosis in a traumatic brain injury model. J. Neurotrauma 30 (1), 55–66 (PubMed PMID: 23046422. Epub 2012/10/11).

Thastrup O, Cullen PJ, Drobak BK, Hanley MR, Dawson AP. Thapsigargin, a tumor promoter, discharges intracellular Ca^{2+} stores by specific inhibition of the endoplasmic reticulum Ca2(+)-ATPase. Proc. Natl. Acad. Sci. U. S. A. 1990 Apr;87(7):2466–2470. (PubMed PMID: 2138778. Pubmed Central PMCID: 53710. (Epub 1990/04/01. eng).

Trendelenburg, G., Dirnagl, U., 2005 Junn. Neuroprotective role of astrocytes in cerebral ischemia: focus on ischemic preconditioning. Glia 50 (4), 307–320 (PubMed PMID: 15846804).

Volmer, R., van der Ploeg, K., Ron, D., 2013 Mar 19. Membrane lipid saturation activates endoplasmic reticulum unfolded protein response transducers through their transmembrane domains. Proc. Natl. Acad. Sci. U. S. A. 110 (12), 4628–4633 (PubMed PMID: 23487760. Pubmed Central PMCID: 3606975).

Wang, H.G., Pathan, N., Ethell, I.M., Krajewski, S., Yamaguchi, Y., Shibasaki, F., et al., 1999 Apr 9. Ca^{2+}-induced apoptosis through calcineurin dephosphorylation of BAD. Science 284 (5412), 339–343 (PubMed PMID: 10195903).

Wang, H., Zhou, C.L., Lei, H., Wei, Q., 2010 Febb. Inhibition of calcineurin by quercetin in vitro and in Jurkat cells. J. Biochem. 147 (2), 185–190 (PubMed PMID: 19880376).

Wang, R., McGrath, B.C., Kopp, R.F., Roe, M.W., Tang, X., Chen, G., et al., 2013 Nov 22. Insulin secretion and Ca^{2+} dynamics in beta-cells are regulated by PERK (EIF2AK3) in concert with calcineurin. J. Biol. Chem. 288 (47), 33824–33836 (PubMed PMID: 24114838. Pubmed Central PMCID: 3837125. Epub 2013/10/12).

Welihinda, A.A., Kaufman, R.J., 1996 Jul 26. The unfolded protein response pathway in *Saccharomyces cerevisiae*. Oligomerization and trans-phosphorylation of Ire1p (Ern1p) are required for kinase activation. J. Biol. Chem. 271 (30), 18181–18187 (PubMed PMID: 8663458. Epub 1996/07/26).

Wu, H.Y., Tomizawa, K., Oda, Y., Wei, F.Y., Lu, Y.F., Matsushita, M., et al., 2004 Feb 6. Critical role of calpain-mediated cleavage of calcineurin in excitotoxic neurodegeneration. J. Biol. Chem. 279 (6), 4929–4940 (PubMed PMID: 14627704).

Yamani, L., Latreille, M., Larose, L., 2014 Marr. Interaction of Nck1 and PERK phosphorylated at Y(5)(6)(1) negatively modulates PERK activity and PERK regulation of pancreatic beta-cell proinsulin content. Mol. Biol. Cell 25 (5), 702–711 (PubMed PMID: 24371088. Pubmed Central PMCID: 3937095).

Zheng, W., Watts, L.T., Holstein, D.M., Prajapati, S.I., Keller, C., Grass, E.H., et al., 2010. Purinergic receptor stimulation reduces cytotoxic edema and brain infarcts in mouse induced by photothrombosis by energizing glial mitochondria. PLoS One 5 (12), e14401 (PubMed PMID: 21203502. Pubmed Central PMCID: 3008710. Epub 2011/01/05. eng).

Zinszner, H., Kuroda, M., Wang, X., Batchvarova, N., Lightfoot, R.T., Remotti, H., et al., 1998 Apr 1. CHOP is implicated in programmed cell death in response to impaired function of the endoplasmic reticulum. Genes Dev. 12 (7), 982–995 (PubMed PMID: 9531536. Pubmed Central PMCID: 316680. Epub 1998/05/09).

Zufferey, R., Nagy, D., Mandel, R.J., Naldini, L., Trono, D., 1997 Sepp. Multiply attenuated lentiviral vector achieves efficient gene delivery in vivo. Nat. Biotechnol. 15 (9), 871–875 (PubMed PMID: 9306402. Epub 1997/11/05).